Neurobiology of Disease

Decreased Neuronal Death in Na^+/H^+ Exchanger Isoform 1-Null Mice after *In Vitro* and *In Vivo* Ischemia

Jing Luo,[1,2] Hai Chen,[2,3] Douglas B. Kintner,[2] Gary E. Shull,[4] and Dandan Sun[1,2]

Departments of [1]Physiology and [2]Neurosurgery and [3]Neuroscience Training Program, University of Wisconsin Medical School, Madison, Wisconsin 53792, and [4]Department of Molecular Genetics, Biochemistry and Microbiology, University of Cincinnati, Cincinnati, Ohio 45267

Na^+/H^+ exchanger isoform 1 (NHE1) is a major acid extrusion mechanism after intracellular acidosis. We hypothesized that stimulation of NHE1 after cerebral ischemia contributes to the disruption of Na^+ homeostasis and neuronal death. In the present study, expression of NHE1 was detected in cultured mouse cortical neurons. Three hours of oxygen and glucose deprivation (OGD) followed by 21 h of reoxygenation (REOX) led to 68 ± 10% cell death. Inhibition of NHE1 with the potent inhibitor cariporide (HOE 642) or genetic ablation of NHE1 reduced OGD-induced cell death by ~40–50% ($p < 0.05$). In NHE1$^{+/+}$ neurons, OGD caused a twofold increase in $[Na^+]_i$, and 60 min REOX triggered a sevenfold increase. Genetic ablation of NHE1 or HOE 642 treatment had no effects on the OGD-mediated initial Na^+_i rise but reduced the second phase of Na^+_i rise by ~40–50%. In addition, 60 min REOX evoked a 1.5-fold increase in $[Ca^{2+}]_i$ in NHE1$^{+/+}$ neurons, which was abolished by inhibition of either NHE1 or reverse-mode operation of Na^+/Ca^{2+} exchange. OGD/REOX-mediated mitochondrial Ca^{2+} accumulation and cytochrome *c* release were attenuated by inhibition of NHE1 activity. In an *in vivo* focal ischemic model, 2 h of left middle cerebral artery occlusion followed by 24 h of reperfusion induced 84.8 ± 8.0 mm^3 infarction in NHE1$^{+/+}$ mice. NHE1$^{+/+}$ mice treated with HOE 642 or NHE1 heterozygous mice exhibited a ~33% decrease in infarct size ($p < 0.05$). These results imply that NHE1 activity disrupts Na^+ and Ca^{2+} homeostasis and contributes to ischemic neuronal damage.

Key words: **oxygen and glucose deprivation; HOE 642; Na^+ and Ca^{2+} accumulation; Na^+/Ca^{2+} exchange; cytochrome *c*; focal ischemia**

Introduction

Na^+/H^+ exchangers (NHEs) catalyze the electroneutral exchange of protons (H^+) and sodium (Na^+) ions across cellular membranes and down their concentration gradients, thereby regulating the pH of the cytoplasm or organellar lumen (Orlowski and Grinstein, 2004; Brett et al., 2005). To date, nine NHE family members have been identified in mammals. NHE1–5 are expressed on the plasma membrane in various cell types. NHE6-9 reside on intracellular organellar membranes of the endosomal/trans-Golgi network (Orlowski and Grinstein, 2004; Brett et al., 2005), although there is evidence that NHE8 is also located on brush border membranes of the renal proximal tubule (Goyal et al., 2005). All of the NHE isoforms share a characteristic secondary structure composed of an NH_2-terminal 10–12 transmembrane ion translocation domain and a large hydrophilic COOH-terminal regulatory domain (Brett et al., 2005).

NHE1 is a ubiquitously expressed plasma membrane protein and the most abundant NHE isoform in the rat CNS (Ma and Haddad, 1997). NHE1 serves the crucial function of protecting cells from internal acidification. In addition to an established role in intracellular pH and cell volume homeostasis, NHE1 can serve as a structural anchor for actin filaments (Denker et al., 2000) and as a plasma membrane scaffold in the assembly of signal complexes that are independent of its function as an ion exchanger (Baumgartner et al., 2004). Therefore, NHE1 may promote signal transduction through diverse effector pathways.

In cardiac myocytes, NHE1 activity has been shown to contribute to the ionic imbalances occurring during ischemia-reperfusion injury. In response to a marked intracellular acidosis and the accumulation of regulatory factors in ischemic heart, NHE1 activity is stimulated to restore pH_i (Avkiran, 2001). The concomitant Na^+ accumulation leads to reversal of the Na^+/Ca^{2+} exchanger and Ca^{2+} overload that ultimately contributes to ischemic cell death in myocardium (Avkiran, 2001).

The role of NHE1 in ion homeostasis in the CNS is not well understood. NHE1 is essential in the maintenance and regulation of pH_i in cortical astrocytes (Mellergard et al., 1993; Shrode and Putnam, 1994; Kintner et al., 2004) and hippocampal neurons (Yao et al., 1999). Our recent study of mouse cortical astrocytes demonstrated that NHE1 activity is significantly elevated after *in vitro* ischemia and leads to overload of intracellular Na^+ and Ca^{2+} (Kintner et al., 2004). Thus, we hypothesized that activation of NHE1 after ischemia may subsequently cause ischemic cerebral damage via Na^+- and Ca^{2+}-mediated toxic effects (Choi, 1995; Brookes et al., 2004). In this study, we investigated whether NHE1 activation after ischemia has a significant impact on the loss of Na^+ and Ca^{2+} homeostasis and on ischemic neuronal cell death.

Received April 27, 2005; revised Oct. 18, 2005; accepted Oct. 20, 2005.

This work was supported in part by National Institutes of Health Grants R01NS38118 and R01NS048216 (D.S.) and R01HL61974 (G.E.S.) and American Heart Association Established-Investigator Award 0540154N (D.S.).

Correspondence should be addressed to Dr. Dandan Sun, Department of Neurological Surgery, University of Wisconsin Medical School, H4/332 Clinical Sciences Center, 600 Highland Avenue, Madison, WI 53792. E-mail: sun@neurosurg.wisc.edu.

DOI:10.1523/JNEUROSCI.3271-05.2005

 0270-6474/05/2511256-13$15.00/0

NHE activity is elevated in hippocampal neurons during either anoxia or reoxygenation (REOX) after hypoxia (Yao et al., 2001; Sheldon and Church, 2002, 2004; Sheldon et al., 2004). Inhibition of NHE activity with nonselective inhibitor EIPA (amiloride derivative ethylisopropylamiloride) or a potent NHE inhibitor SM-20220 (*N*-aminoiminomethyl-1-methyl-1-indole-2-carboxamide methanesulfonate) significantly reduces loss of gerbil CA1 pyramidal neurons after global ischemia (Phillis et al., 1999) and the increase in rat brain Na^+ and water content after focal ischemia (Kuribayashi et al., 1999).

In this study, we used both a pharmacological approach, using the potent NHE1 inhibitor cariporide (HOE 642), and genetic ablation of NHE1 to elucidate the function of NHE1 in ischemic neuronal cell damage. We report here that inhibition of NHE1 activity reduced neuronal cell death in both *in vitro* and *in vivo* ischemic models, thereby showing that NHE1 activity contributes to the perturbations of Na^+ and Ca^{2+} homeostasis in cerebral ischemia.

Materials and Methods

Materials. Eagle's modified essential medium (EMEM) and HBSS were obtained from Mediatech Cellgro (Herndon, VA). Fetal bovine serum (FBS) and horse serum (HS) were obtained from Hyclone Laboratories (Logan, UT). The acetoxymethyl esters of 2′,7′-bis(2-carboxyethyl)-5,6-carboxyfluorescein (BCECF-AM), 1-[6-amino-2-(5-carboxy-2-oxazolyl)-5-benzofuranyloxy]-2-(2-amino-5-methylphenoxy)ethane-*N*,*N*,*N*′,*N*′-tetraacetic acid (fura-2 AM), and sodium-binding benzofuran isophthalate (SBFI-AM) were obtained from Invitrogen (Eugene, OR). Pluronic acid was purchased from BASF (Ludwigshafen, Germany). Nigericin, monensin, carbonyl cyanide *p*-trifluoromethoxyphenylhydrazone (FCCP), oligomycin, thapsigargin, and gramicidin were purchased from Sigma (St. Louis, MO). HOE 642 was a kind gift from Aventis Pharma (Frankfurt, Germany). G116 antibody was a kind gift from Dr. Leong L. Ng (University of Leicester, Leicester, UK). SEA0400 [(2-[4-[2,5-diflurophenyl) methoxy]phenoxy]-5-ethoxyaniline] was from EMD Biosciences (San Diego, CA). Antibody for β tubulin type-III was obtained from Promega (Madison, WI), and anti-cytochrome *c* antibody (clone 6H2.B4) was obtained from PharMingen (San Jose, CA).

Cortical neuron cultures. NHE1 null mutant ($NHE1^{-/-}$) mice were established previously (Bell et al., 1999). Male and female heterozygous mutant ($NHE1^{+/-}$) mice were paired for 48 h and then separated. As described in our recent study (Chen et al., 2005), embryonic day 14 (E14) to E16 pregnant mice were anesthetized with 5% halothane and killed. Fetuses were removed and rinsed in cold HBSS. Each mouse fetus was genotyped. The tails were removed from the fetus, and PCR was performed as described previously (Kintner et al., 2004).

The cortices were removed and minced as described previously (Beck et al., 2003). The tissues were treated with 0.2 mg/ml trypsin at 37°C for 25 min. The cells were centrifuged at 350 g for 4 min. The cell suspension was diluted in EMEM containing 5% FBS and 5% HS. The cells from individual fetal cortices were seeded separately in 24-well plates or on glass coverslips coated with poly-D-lysine and incubated at 37°C in an incubator with 5% CO_2 and atmospheric air. After 96 h in culture, 1 ml of fresh media containing 8 μM cytosine 1-b-D-arabinofuranoside was added. The media were replaced as described previously (Chen et al., 2005). Cultures 10–15 days in culture (DIV) were used in the study.

Oxygen and glucose deprivation treatment. Ten to 15 DIV neuronal cultures were rinsed with an isotonic oxygen and glucose deprivation (OGD) solution, pH 7.4, containing the following (in mM): 0 glucose, 20 $NaHCO_3$, 120 NaCl, 5.36 KCl, 0.33 Na_2HPO_4, 0.44 KH_2PO_4, 1.27 $CaCl_2$, and 0.81 $MgSO_4$. Cells were incubated in 0.5 ml of the OGD solution in a hypoxic incubator (model 3130; Thermo Forma, Marietta, OH) containing 94% N_2, 1% O_2, and 5% CO_2. The oxygen level in the medium of cultured cells in 24-well plates was monitored with an oxygen probe (model M1–730; Microelectrodes, Bedford, NH) and decreased to ~2–3% after 60 min in the hypoxic incubator. The OGD incubation was 3 h for cell viability assay. For REOX, the cells were incubated for 21 h in 0.5 ml of EMEM containing 5.5 mM glucose at 37°C in the incubator with 5% CO_2 and atmospheric air. In our pilot studies, no significant differences were found in the neuronal toxicity assay after 2 h OGD/22 h REOX versus 3 h OGD/21 h REOX. For ionic measurements, the OGD incubation was 2 h in the hypoxic incubator, and REOX was performed on the microscope stage (in an open chamber with a buffer change every 10 min).

Normoxic control cells for cell viability assay were incubated for 3 h in 5% CO_2 and atmospheric air in a buffer identical to the OGD solution except for the addition of 5.5 mM glucose. After 3 h, the normoxic buffer was replaced with normal EMEM and cells were incubated for another 21 h. In the drug treatment studies, cells were pretreated with 1 μM HOE 642 for 30 min and the drug remained present in all subsequent incubations and washes.

Measurement of cell death. Cell viability was assessed by propidium iodide (PI) uptake and retention of calcein using a Nikon TE 300 inverted epifluorescence microscope. Cultured neurons were rinsed with HEPES-MEM and incubated with 1 μg/ml calcein-AM and 10 μg/ml PI in the same buffer at 37°C for 30 min. The composition of HEPES-MEM was described previously (Su et al., 2002). For cell counting, cells were rinsed with the isotonic control buffer and visualized using a Nikon (Tokyo, Japan) 20× objective lens. Calcein and PI fluorescence were visualized using FITC filters and Texas Red filters as described previously (Beck et al., 2003). Images were collected using a Princeton Instruments (Trenton, NJ) MicroMax CCD camera. In a blind manner, a total of 1000 cells/condition were counted using MetaMorph image-processing software (Universal Imaging, Downingtown, PA). Cell mortality was expressed as the ratio of PI-positive cells to the sum of calcein-positive and PI-positive cells.

Intracellular Na^+ measurement. Intracellular Na^+ concentration ($[Na^+]_i$) was measured with the fluorescent dye SBFI-AM as described previously (Kintner et al., 2004). Cultured neurons grown on coverslips were loaded with 10 μM SBFI-AM plus 0.05% pluronic acid during 2 h of OGD. In our pilot study, OGD (2 h) did not significantly decrease retention of calcein fluorescence signal and fluorescent intensity of either pH indicator BCECF, Na^+ dye SBFI, or Ca^{2+} dye fura-2. Therefore, SBFI-AM and fura-2 AM were loaded during OGD throughout this study.

The coverslips were placed in an open-bath imaging chamber (model RC24; Warner Instruments, Hamden, CT) containing HEPES-MEM at ambient temperature. Using a Nikon TE 300 inverted epifluorescence microscope and a 40× lens, neurons were excited every 30 s at 345 and 385 nm and the emission fluorescence at 510 nm recorded. Images were collected and the 345/385 ratios analyzed with the MetaFluor image-processing software as described previously (Su et al., 2002). At the end of each experiment, absolute $[Na^+]_i$ was determined for each cell by performing an *in situ* calibration as described previously (Su et al., 2002).

Because severe phototoxicity and excitotoxicity were observed in neurons at 37°C, in the current study, all intracellular Na^+ (except Fig. 4*D*) as well as pH_i and Ca^{2+} measurements were performed at room temperature. Similar Na^+ values under control and excitotoxic conditions were found in ambient temperature and 37°C (Beck et al., 2003). To further reduce imaging-induced phototoxicity, the HEPES-MEM was supplemented with the following (in mM): 1.0 pyruvate, 0.4 ascorbic acid, 0.01 troloxC, and 0.1 butylated hydroxyanisole (Dent et al., 1999). The supplement was present during imaging of all normoxic control and experimental neurons in 60 min REOX. High concentrations of Trolox C have been shown to prevent lipid peroxidation (IC_{50}, ~30–100 μM), neurotoxicity (100–750 μM), and reduce Na^+ influx (200–1000 μM) (Sheldon et al., 2004; Kraus et al., 2005). In our study, we used a low concentration and short exposure of Trolox C to minimize its broader neuroprotective functions. In addition, the supplements had no neuroprotection on cell mortality during 3 h of OGD and 21 h of REOX (data not shown).

Measurement of pH_i. pH_i measurement and prepulse treatment were performed at room temperature as described previously (Kintner et al., 2004). Briefly, neurons grown on coverslips were incubated for 10 min with 2.5 μM BCECF-AM in HEPES-buffered solution at ambient temperature. The coverslips were then washed and placed in the open-bath

imaging chamber. The chamber was mounted on the stage of the TE 300 inverted epifluorescence microscope, and the neurons were visualized. The cells in the buffer supplemented with anti-oxidants were excited every 10–30 s at 440 and 490 nm, and the emission fluorescence at 535 nm was recorded. Images were collected using a Princeton Instruments MicroMax CCD camera and analyzed with MetaFluor image-processing software. The ratio of the fluorescence emissions (F_{490}/F_{440}) was calibrated using the high K^+/nigericin technique (Boyarsky et al., 1993).

NH_4^+/NH_3 solutions were prepared by replacing 10 mM NaCl in the HEPES-buffered solution with an equimolar concentration of NH_4Cl. pH_i recovery was determined during the first min after NH_4^+/NH_3 prepulse from the slope of a fitted linear regression (Kintner et al., 2004).

Intracellular Ca^{2+} measurement. Neurons grown on coverslips were incubated with 5 μM fura-2 AM during 2 h of OGD treatment. After OGD, the cells were washed with HEPES-MEM and the coverslips were placed in the open-bath imaging chamber containing HEPES-MEM with the antioxidant supplement at ambient temperature. Using a Nikon TE 300 inverted epifluorescence microscope and a 40× objective lens, neurons were excited every 10 min at 345 and 385 nm, and the emission fluorescence at 510 nm was recorded. Images of cells (~20/field) were collected and analyzed with the MetaFluor image-processing software. At the end of each experiment, the cells were exposed to 1 mM $MnCl_2$ in Ca^{2+}-free HEPES-MEM. The Ca^{2+}-insensitive fluorescence was subtracted from each wavelength before calculations (Lenart et al., 2004). The $MnCl_2$-corrected 345/385 emission ratios were converted to concentration as described in our previous study (Lenart et al., 2004).

To monitor Ca^{2+} release from mitochondria, FCCP (10 μM) and oligomycin (2.5 μg/ml) were applied to collapse the mitochondria membrane potential and to block F_1F_0-ATP synthase.

Immunofluorescence staining. Cultured cells grown on coverslips were rinsed with PBS, pH 7.4, and fixed with 4% paraformaldehyde in PBS (Kintner et al., 2004). After rinsing, cells were incubated with blocking solution (10% normal goat serum, 0.4% Triton X-100, and 1% bovine serum albumin in PBS) for 1 h. Cells were incubated with anti-NHE1 polyclonal antibody (G116, 1:100) plus anti-βIII tubulin monoclonal antibody (1:200) for 1 h at 37°C, followed by overnight incubation at 4°C. After rinsing in PBS, cells were incubated with goat anti-mouse fluorescein isothiocyanate-conjugated IgG (1:100; Sigma) and goat anti-rabbit Texas Red-X conjugated IgG (1:100; Invitrogen) for 1 h at 37°C. Fluorescence images were captured by the Nikon TE 300 inverted epifluorescence microscope (20×) using a Princeton Instruments MicroMax CCD camera and MetaMorph image-processing software. Identical digital imaging acquisition parameters were used in both negative control and experimental images.

Cytochrome c *immunofluorescence.* Colocalization of cytochrome *c* (Cyt C) release and neuronal death was determined with PI staining in conjunction with a specific antibody staining against Cyt C (Pei et al., 2003). Briefly, cells on coverslips were first stained with 5 μM PI for 5 min and washed with PBS three times. They were fixed in 4% paraformaldehyde in PBS for 10 min. After rinsing, cells were incubated with the blocking solution for 20 min followed by the application of the anti-Cyt C antibody (1:100 diluted in blocking buffer) for 1 h at room temperature. After rinsing in PBS, coverslips were incubated with goat anti-mouse fluorescein isothiocyanate-conjugated IgG (1:100) for 1 h at 37°C. Fluorescence images were captured by the Nikon TE 300 inverted epifluorescence microscope (60×) using a Princeton Instruments MicroMax CCD camera and MetaMorph image-processing software.

Quantitation of Cyt C release from mitochondria. Cyt C release in the cytosol was assessed after subcellular fraction preparation. The culture medium was removed from the plates, and cells were incubated in 2 ml of Trypsin (0.2 mg/ml)-EDTA (1 mM) solution at 37°C for 10 min. The cells were detached and cell suspension was prepared in 5 ml of EMEM. After centrifugation of the cell suspension at 500 g for 5 min, the pellet was resuspended in 100 μl lysis buffer, pH 7.4, which contained the following (in mM): 18.3 NaH_2PO_4, 146 NaCl, 85.9 Na_2HPO_4, 250 sucrose, 2 EDTA, 0.081 digitonin, and a protease inhibitor mixture as described previously (Kintner et al., 2004). After 5 min of incubation, the cell lysate was centrifuged for 10 min at 750 × *g* at 4°C, and the pellets containing the nuclei and unbroken cells were discarded. The supernatant was then centrifuged at 15,000 × *g* for 15 min. The resulting supernatant was removed and used as the cytosolic fraction. The pellet fraction containing mitochondria was further incubated with PBS containing 0.5% Triton X-100 for 10 min at 4°C. After centrifugation at 16,000 × *g* for 10 min, the supernatant was collected as mitochondrial fraction. Protein content was determined by bicinchoninic acid method (Kintner et al., 2004). The levels of Cyt C in cytosolic and mitochondrial fractions were measured using the Quantikine M Rat/Mouse Cytochrome C Immunoassay kit (R&D Systems, Minneapolis, MN).

Gel electrophoresis and Western blotting. Cells were scraped from the plates and lysed in PBS, pH 7.4, containing 2 mM EDTA and protease inhibitors by 30 s sonication at 4°C (Kintner et al., 2004). Protein content was determined as above. Protein samples (15 μg/lane) and prestained molecular mass markers (Bio-Rad, Hercules, CA) were denatured in SDS reducing buffer (1:2 by volume; Bio-Rad). The samples were then electrophoretically separated on 6% SDS gels, and the resolved proteins were electrophoretically transferred to a polyvinylidene difluoride membrane (Kintner et al., 2004). The blots were incubated in 7.5% nonfat dry milk in Tris-buffered saline (TBS) overnight at 4°C and then incubated for 1 h with a primary antibody. The blots were rinsed with TBS and incubated with horseradish peroxidase-conjugated secondary IgG for 1 h. Bound antibody was visualized using the enhanced chemiluminescence assay (Amersham Biosciences, Piscataway, NJ).

Polyclonal G116 antibody against NHE1 (1:1000) (Kelly et al., 1997) and anti-β tubulin monoclonal antibody (1:3000) were used for detection of NHE1 and β tubulin (type-III), respectively.

Animal preparation. $NHE1^{+/+}$ adult mice (SV129/Black Swiss; 20–25 g) were anesthetized with 5% halothane for induction and 0.8–1.0% halothane plus N_2O and O_2 (3:2) for maintenance. The left femoral artery was cannulated for blood pressure monitoring and sampling. Blood samples (80–100 μl) were taken before and during 1 h ischemia for analysis of P_aO_2, P_aCO_2, pH, Na^+, and K^+ with an i-STAT analyzer (i-STAT, East Windsor, NJ). The normal volume was maintained by injection of isotonic saline. Rectal temperatures were monitored and maintained at 37.0 ± 0.5°C with a heating blanket and a heating lamp. In a separate set of animals, tympanic membrane temperature was measured with an infrared thermometer (Thermoscan IRT 4020; Braun, Kronberg, Germany). Regional cerebral blood flow (CBF) was measured with a laser Doppler probe as described previously (Chen et al., 2005). All of the mice underwent 2 h of middle cerebral artery (MCA) occlusion (MCAO) ischemia and subsequent 24 h reperfusion.

Focal ischemia model and drug administration. Focal cerebral ischemia in mice was induced by occlusion of the left MCA, as described previously (Chen et al., 2005). Briefly, the left common carotid artery was exposed and the occipital artery branches of the external carotid artery (ECA) were isolated and coagulated. After coagulation of the superior thyroid artery, the ECA was dissected and coagulated. The internal carotid artery (ICA) was isolated and the extracranial branch of the ICA was then dissected and ligated. A polyamide resin glue-coated suture (6–0 monofilament nylon) was introduced into the ECA lumen and then advanced ~9–9.5 mm in the ICA lumen to block the MCA blood flow. The suture was withdrawn 2 h after MCAO. The incision was closed and the mice recovered under a heating lamp to ensure that the core temperature (36.0 ± 0.6°C) was maintained during recovery. After recovery, animals were returned to their cages with free access to food and water. At 24 h of reperfusion, the animals were killed for infarction and brain water content measurements. For NHE1 inhibitor HOE 642 treatment, 1 mg/kg HOE 642 in saline was administered through the left femoral vein 5 min before the MCAO induction.

A total of 64 adult mice (20–25 g of body mass) were used in this study. Five mice died because of perforated intracranial vessels by nylon sutures and excluded from the study. All animal procedures used in this study were conducted in strict compliance with the National Institutes of Health *Guide for the Care and Use of Laboratory Animals* and approved by the University of Wisconsin Center for Health Sciences Research Animal Care Committee.

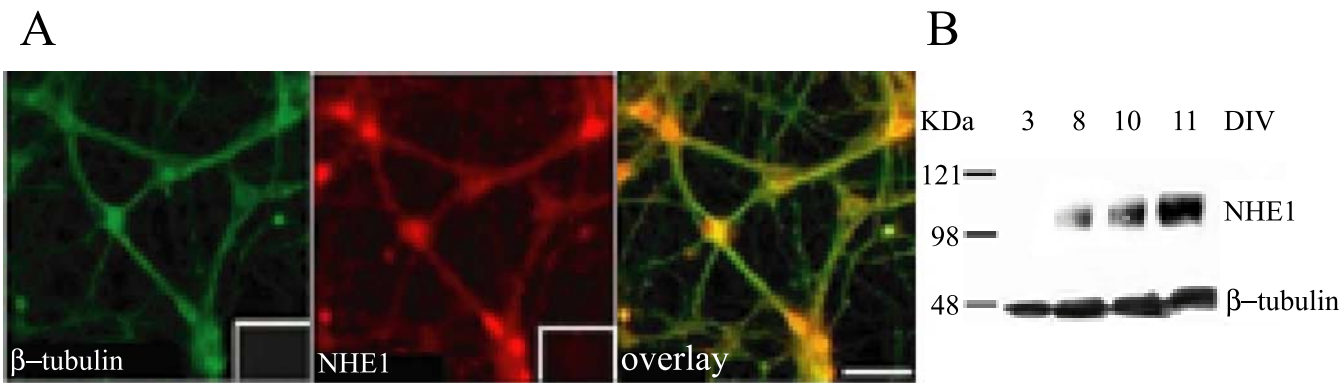

Figure 1. Expression of NHE1 in cultured cortical neurons. ***A***, Immunofluorescence staining of neurons in primary cultures (11–15 DIV). Left, Anti-tubulin (β-III) antibody staining. Middle, NHE1 staining. Right, Overlay images of the left and middle panels. Scale bar, 25 μm. Insets, Omission of the primary antibodies. ***B***, Development-dependent expression of NHE1 in neuronal cultures. Cellular lysates were separated electrophoretically as described in Materials and Methods. Expression of NHE1 and βIII-tubulin protein in cultures at 3–11 DIV is shown on the same blot.

Infarction size measurement. After 24 h of reperfusion, saline-treated control NHE1 $^{+/+}$ mice, HOE 642-treated NHE1 $^{+/+}$ mice, or NHE1 $^{+/-}$ mice were anesthetized with 5% halothane plus N_2O and O_2 (3:2) and then decapitated. As described in our previous study (Chen et al., 2005), 2 mm coronal slices were made and stained for 20 min at 37°C with 2% 2, 3, 5,-triphenyltetrazolium chloride monohydrate (TTC). Infarction volume was calculated using NIH image analysis software as described by Swanson et al. (1990). Brain swelling in the ischemic hemisphere was taken into consideration during the analysis. Infarction areas on each section were summed and multiplied by section thickness to give the infarction volume.

Water content measurement. After 24 h of reperfusion, control and HOE 642-treated NHE1 $^{+/+}$ mice were decapitated under deep anesthesia with 5% halothane plus N_2O and O_2 (3:2). The ipsilateral and contralateral hemispheres were dissected, and wet weight of the tissue was measured. The tissue was dried at 120°C for 24 h. The hemispheric water content was calculated as the difference between wet and dry weights and expressed as a percentage of wet weight.

Statistical analysis. Values are presented as mean ± SD (Figs. 3, 7–9) and mean ± SE (Figs. 2, 4, 5). Comparisons of means were performed between groups by the nonparametric Mann–Whitney test. A linear regression was fitted and compared by an F-statistic test for comparison of slopes. A p value of <0.05 was considered statistically significant.

Results

Expression of NHE1 in neurons

As shown in Figure 1*A* (left), NHE1 $^{+/+}$ neurons in primary cultures were identified by immunofluorescence staining for the neuronal marker βIII tubulin. NHE1 expression was localized in both soma and neurite processes (Fig. 1*A*, middle). Colocalization of NHE1 and tubulin was found in all neurons (Fig. 1*A*, right).

Expression of NHE1 protein in NHE1 $^{+/+}$ neuronal cultures was examined by immunoblotting (Fig. 1*B*). Lysates of cultured cells (3–11 DIV) were probed for expression of NHE1 and βIII-tubulin proteins. No NHE1 protein was detected at 3 DIV, but a protein band of ~110 kDa gradually increased at 8 and 10 DIV. At 11 DIV, neuronal cultures expressed abundant NHE1 protein, which is consistent with the immunofluorescence staining data (shown above). Inability to detect NHE1 protein at 3 DIV is not attributable to insufficient protein loading. On the same blot, expression of βIII-tubulin was readily seen at 3 DIV and throughout 8–11 DIV. A development-dependent expression of NHE1 has also been seen *in vivo* at postnatal day 1 (P1) and P13 (Douglas et al., 2001). Given 21 d of gestation in mice, the age of 8–11 DIV neuronal cultures would be similar to one in P2–P5 mice.

Because the neuronal-enriched cultures used in this study contained ~10–15% astrocytes, the immunoreactive signals of NHE1 in the immunoblot represent expression of NHE1 protein from both neurons and astrocytes.

NHE1 is important in pH_i regulation after intracellular acidosis

We then investigated whether inhibition of NHE1 activity with the potent NHE1 inhibitor HOE 642 affects pH_i regulation in NHE1 $^{+/+}$ cortical neurons. As shown in Figure 2*A*, when a NHE1 $^{+/+}$ neuron was exposed to 10 mM NH_3/NH_4, pH_i rose rapidly as NH_3 diffused into the cell and combined with H^+ to form NH_4^+ (Fig. 2*Aa*,*b*). As the cell was returned to the standard HCO_3^--free HEPES-buffered solution, pH_i decreased sharply as NH_4 rapidly left the cell as NH_3, trapping H^+ inside (Fig. 2*Ab*,*c*). After the acid load, pH_i recovered within 5 min (Fig. 2*Ac*,*d*). To test whether NHE1 functions in H^+ extrusion and pH_i recovery, the cell was subsequently exposed to 1 μM HOE 642, which decreased resting pH_i (Fig. 2*Ad*,*e*). A second NH_3/NH_4^+ prepulse (Fig. 2*Ae*,*f*) triggered a sudden decrease in pH_i, and pH_i recovery was blocked by HOE 642 (Fig. 2*Ag*,*h*).

Basal pH_i in cortical NHE1 $^{+/+}$ neurons was 7.14 ± 0.04 (Fig. 2*D*). Inhibition of NHE1 activity with HOE 642 significantly reduced basal pH_i to 6.93 ± 0.04 ($p < 0.05$). In response to acidosis, NHE1 $^{+/+}$ neurons exhibited a fast pH_i recovery with a 0.28 ± 0.02 pH U/min rate (at a mean pH_i of 6.64 ± 0.03) (Fig. 2*A*,*E*). pH_i returned to the basal level in 3.49 ± 0.60 min in NHE1 $^{+/+}$ neurons. In contrast, when NHE1 activity was blocked by HOE 642, pH_i recovery rate decreased to 0.02 ± 0.01 pH U/min (at a mean pH_i of 6.58 ± 0.04; $p < 0.05$) (Fig. 2*A*,*E*) and pH_i failed to return to the basal level during the ~15 min recovery time.

H^+ extrusion and pH_i recovery were also reduced in NHE1 $^{+/-}$ neurons (Fig. 2*B*). After acidosis, pH_i recovery rate was 0.17 ± 0.06 pH U/min in NHE1 $^{+/-}$ neurons (at a mean pH_i of 6.66 ± 0.05) (Fig. 2*B*,*E*), a ~40% of reduction compared with NHE1 $^{+/+}$ neurons. Inhibition of NHE1 with HOE 642 caused an additional decrease of H^+ extrusion in NHE1 $^{+/-}$ neurons. This indicates that NHE1 $^{+/-}$ neurons indeed express less NHE1 activity.

NHE1 $^{-/-}$ neurons exhibited a reduced basal pH_i (7.03 ± 0.02) (Fig. 2*C*,*D*). There was no pH recovery after the acidosis in NHE1 $^{-/-}$ neurons (Fig. 2*C*). NHE1 $^{-/-}$ neurons had an initial pH_i recovery rate of only 0.04 ± 0.01 pH U/min (at a mean pH_i of 6.52 ± 0.06; $p < 0.05$) (Fig. 2*E*) and exhibited no significant pH_i

recovery after acidification. Together, these data suggest that NHE1 is involved in maintenance of resting pH_i in cortical neurons and plays an essential role in acid extrusion after acidosis.

Inhibition of NHE1 activity significantly reduces OGD-induced cell death

A low level of cell death occurred in control NHE1$^{+/+}$ neurons (Fig. 3*A*,*B*). After 3 h of OGD and 21 h of REOX, NHE1$^{+/+}$ neurons exhibited a significant increase in cell death (68 ± 10%; $p < 0.05$) (Fig. 3*C*,*D*,*G*) compared with basal levels of cell death under normoxic conditions. In contrast, inhibition of NHE1 activity with 1 μM HOE 642 significantly attenuated OGD-mediated cell death in NHE1$^{+/+}$ neurons (33 ± 14%; $p < 0.05$) (Fig. 3*E*,*F*,*G*). This finding suggests that NHE1 plays a role in ischemic neuronal damage.

To further confirm that NHE1 activity contributes to ischemic neuronal death after OGD, we also investigated whether NHE1$^{+/-}$ and NHE1$^{-/-}$ neurons exhibit less cell damage. As shown in Figure 3*G*, compared with the ~70% cell death observed in NHE1$^{+/+}$ neuron cultures, NHE1$^{-/-}$ and NHE1$^{+/-}$ neurons exhibited a significant reduction in OGD-mediated cell death (41 ± 13 and 50 ± 7%, respectively; $p < 0.05$). No additional neuroprotection was found when NHE1$^{-/-}$ neuron cultures were exposed to 1 μM HOE 642 (42 ± 15%; $p > 0.05$) (Fig. 3*G*). Although the cell death rate was slightly higher in HOE 642-treated NHE1$^{-/-}$ neurons, it was not significantly different from that of HOE 642-treated NHE1$^{+/-}$ or NHE1$^{+/+}$ neurons. This finding further supports our hypothesis that NHE1 plays a role in ischemic neuronal damage.

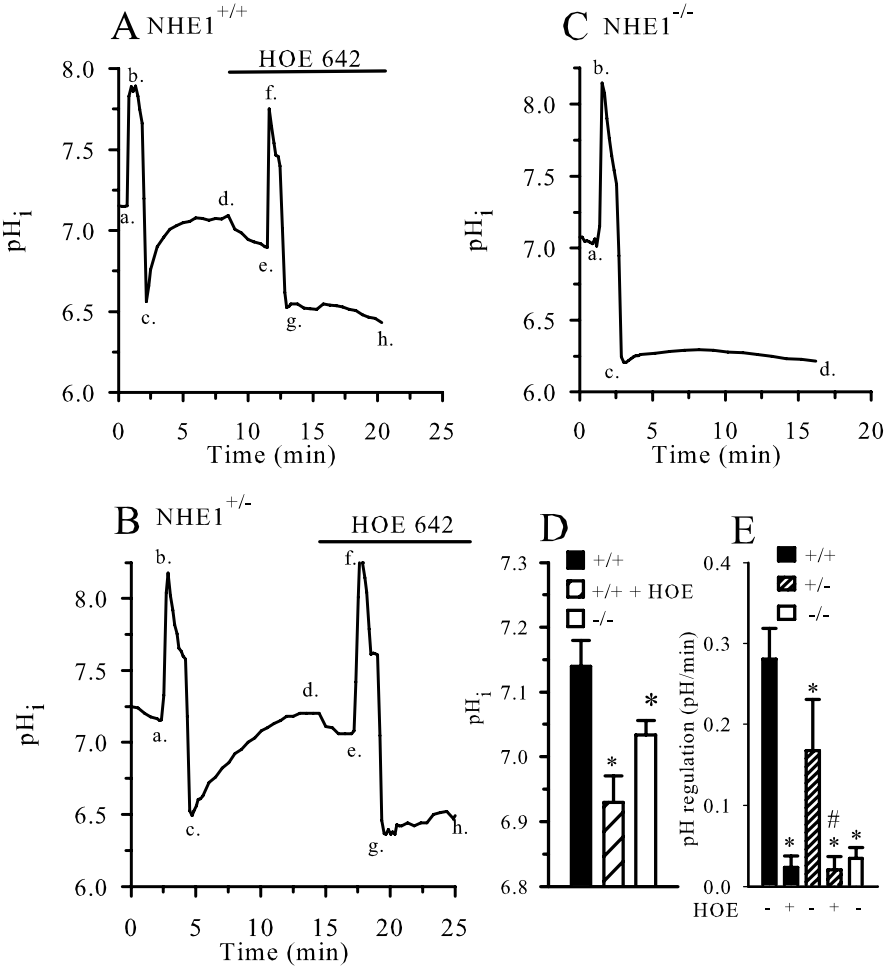

Figure 2. Inhibition of NHE1 affects pH_i regulation in cortical neurons. ***A***, A representative trace of pH_i from a NHE1$^{+/+}$ neuron. After 2 min of baseline (***a***, ***b***), the cells were exposed to 10 mM NH_3/NH_4^+ for 1 min (***b***, ***c***) and then returned to standard HEPES-buffered solution, and pH_i recovered (***c***, ***d***). After the pH_i plateaued, the cells were exposed to 1 μM HOE 642 in HEPES-buffered solution, and a new basal pH_i was established (***d***, ***e***). The cell was then exposed to a second NH_4^+-prepulse (***f***, ***g***), and pH_i recovery rate was monitored (***g***, ***h***). ***B***, ***C***, A representative trace of pH_i from a NHE1$^{+/-}$ (***B***) or NHE1$^{-/-}$ (***C***) neuron in response to a similar protocol as in ***A***. ***D***, ***E***, Summary of the change in basal pH_i (***D***) and pH_i recovery rate (***E***) after acidification. Data are expressed as mean ± SE ($n = 4$–13). $^*p < 0.01$ versus +/+; $^\#p < 0.01$ versus +/− without HOE.

NHE1$^{-/-}$ neurons or NHE1$^{+/+}$ neurons treated with HOE 642 reduce the second phase of Na^+ rise during reoxygenation

We hypothesized that NHE1 contributes to ischemic cell death in part via intracellular Na^+ loading. To further investigate the role of NHE1 in the change of Na^+ homeostasis, cells were exposed to 2 h of OGD, and $[Na^+]_i$ was monitored at the end of OGD and at 10 min intervals during 60 min REOX (Fig. 4*A*–*D*). Two hours of OGD caused a small but significant increase in $[Na^+]_i$ in NHE1$^{+/+}$ neurons (16.2 ± 4.5 mM). NHE1$^{-/-}$ neurons and HOE 642-treated NHE1$^{+/+}$ neurons had similar degrees of increase in $[Na^+]_i$ (14.8 ± 1.3 and 12.2 ± 0.7 mM, respectively). Although inhibition of NHE1 activity appeared to reduce the $[Na^+]_i$ at the end of 2 h of OGD, the changes were not statistically significant ($p = 0.66$ and $p = 0.28$, respectively). These data show that loss of NHE1 activity did not affect the OGD-mediated rise in $[Na^+]_i$. Other possible mechanisms contributing to the Na^+ entry are discussed in Discussion.

After REOX, $[Na^+]_i$ rose at a rate of 0.47 ± 0.02 mM/min in NHE1$^{+/+}$ neurons, which was significantly accelerated compared with normoxic control cells (0.08 ± 0.01 mM/min) (Fig. 4*A*). At the end of 60 min REOX, $[Na^+]_i$ increased to 43.3 ± 3.0 mM in NHE1$^{+/+}$ neurons. In contrast, the OGD-induced rise in $[Na^+]_i$ was significantly slower in NHE1$^{-/-}$ neurons (0.20 ± 0.01 mM/min; $p < 0.05$) (Fig. 4*B*) or in NHE1$^{+/+}$ neurons treated with HOE 642 (0.15 ± 0.01 mM/min; $p < 0.05$) (Fig. 4*C*). At 60 min REOX, $[Na^+]_i$ was only 25.9 ± 1.3 mM in NHE1$^{-/-}$ neurons and 20.5 ± 1.3 mM in NHE1$^{+/+}$ neurons treated with HOE 642. A linear regression was fit to the changes in $[Na^+]_i$, and the slope in NHE1$^{+/+}$ neurons was significantly different from those of NHE1$^{-/-}$ neurons or NHE1$^{+/+}$ neurons treated with HOE 642 (Fig. 4*A*–*C*). The rates of increase in Na^+_i were not different between NHE1$^{-/-}$ neurons and NHE1$^{+/+}$ neurons plus HOE 642 ($p > 0.05$); however, they were still higher than those observed under normoxic control conditions ($p < 0.001$) (Fig. 4*A*–*C*). Moreover, Na^+_i rise was irreversible and no recovery was found at 3 h REOX (data not shown). These findings suggest that NHE1 activation is in part responsible for the Na^+ overload in neurons during reoxygenation.

To further verify the role of NHE1 in Na^+ overload, similar

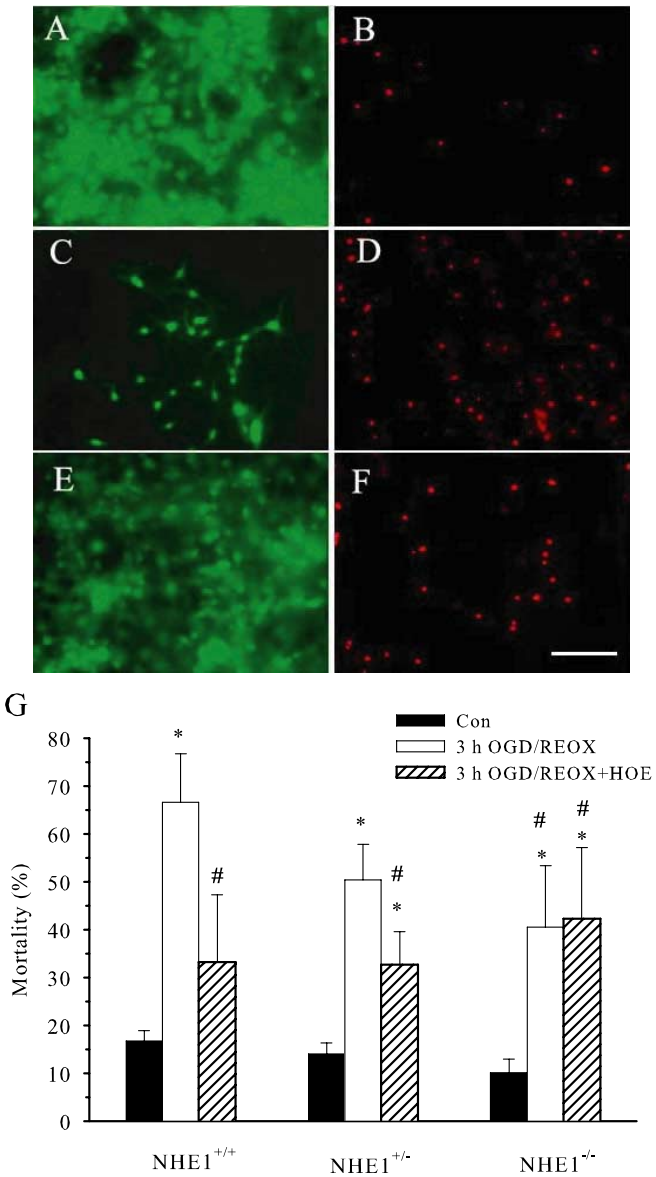

Figure 3. Inhibition or ablation of NHE1 activity abolishes OGD-mediated cell death. Cell mortality was assessed in 12–15 DIV cortical neurons after 3 h of OGD and 21 h of REOX. For HOE 642 treatment, NHE1 $^{+/+}$ neurons were incubated in the presence of 1 μM HOE 642 at 37°C for 3 h of OGD and 21 h of REOX. Sister NHE1 $^{+/+}$ cultures were incubated for 24 h in normoxic control buffers (Con). Similar assays were also performed in NHE1 $^{+/-}$ and NHE1 $^{-/-}$ cultures. At the end of the experiment, cells were stained with PI and calcein-AM, and cell images were acquired. ***A***, ***C***, ***E***, Calcein-AM. ***B***, ***D***, ***F***, PI. ***A***, ***B***, Con. ***C–F***, OGD/REOX. ***E***, ***F***, OGD/REOX plus HOE. Scale bar, 256 μm. ***G***, Summary data. Data are means ± SD ($n = 5–8$ cultures). *$p < 0.05$ versus Con; $^{\#}p < 0.05$ versus NHE1 $^{+/+}$ OGD/REOX. Error bars represent SD.

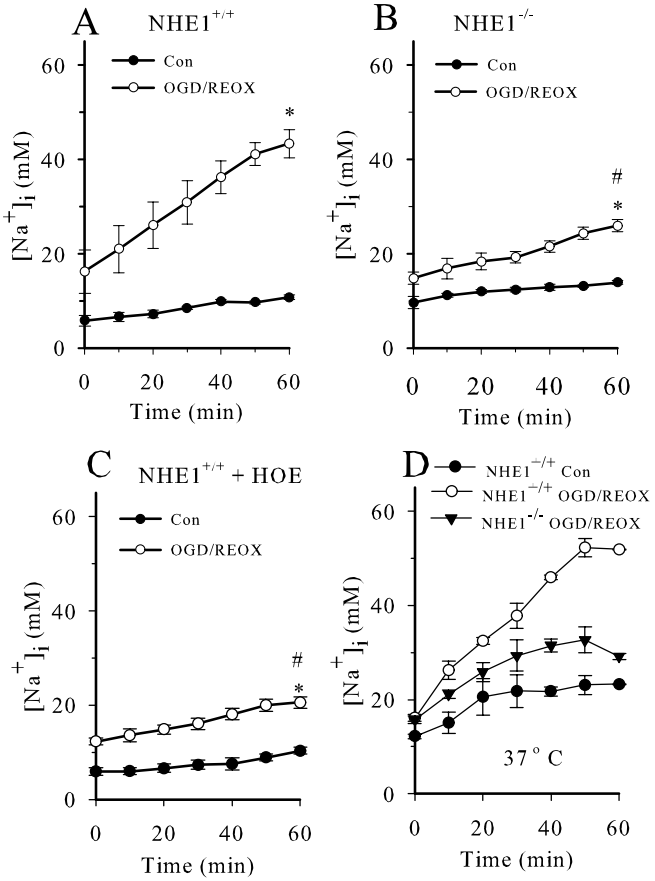

Figure 4. Inhibition of NHE1 attenuates Na^+_i rise during reoxygenation. $[Na^+]_i$ in NHE1 $^{+/+}$, NHE1 $^{-/-}$, or NHE1 $^{+/+}$ neurons treated with 1 μM HOE 642 were measured with SBFI immediately after 2 h of OGD and every 10 min for 1 h. Normoxic controls (Con) were done in sister cultures after 3 h of incubation in normoxic control buffers. ***A–C***, HCO_3^--free buffers at room temperature. ***D***, HCO_3^--containing buffer (26 mM) at 37°C. Data are means ± SE ($n =$ 3–4 cultures). *$p < 0.001$ versus Con (linear regressions); $^{\#}p < 0.001$ versus NHE1 $^{+/+}$ OGD/REOX (linear regressions).

experiments were performed at more physiological conditions (37°C and in the presence of HCO_3^-). As shown in Figure 4*D*, Na^+ rise in NHE1 $^{+/+}$ neurons was accelerated (1.0 mM/min) after 2 h of OGD and reached 52 ± 0.1 mM at 60 min REOX. In contrast, NHE1 $^{-/-}$ neurons exhibited significantly less Na^+ accumulation (0.54 mM/min). The amount of Na^+ accumulation via NHE1 was similar at room temperature versus 37°C. This differs from the reports that NHE activity is reduced at room temperature in myocytes and acutely isolated rat hippocampal neurons (Sheldon and Church, 2002; Ch'en et al., 2003). No HCO_3^--dependent compensatory effects were found in NHE1 $^{-/-}$ neurons.

Inhibition of NHE1 activity blocks OGD/REOX-mediated increase in $[Ca^{2+}]_i$

In addition to Na^+ homeostasis, we speculated that NHE1-mediated Na^+ loading would indirectly affect Ca^{2+} levels. $[Ca^{2+}]_i$ was determined in NHE1 $^{+/+}$ neurons every 10 min during 1 h of REOX after 2 h of OGD (Fig. 5*A*). $[Ca^{2+}]_i$ in NHE1 $^{+/+}$ neurons was 61 ± 10 nM under normoxic control conditions. There was a small change in $[Ca^{2+}]_i$ in normoxic NHE1 $^{+/+}$ neurons at a rate of 0.6 nM/min over time. $[Ca^{2+}]_i$ reached 95 ± 4 nM at the end of the normoxic incubation. Two hours of OGD did not significantly change $[Ca^{2+}]_i$ (62 ± 14 nM). Likewise, $[Ca^{2+}]_i$ remained unchanged in NHE1 $^{+/+}$ neurons treated with HOE 642 (54 ± 8 nM) or in NHE1 $^{-/-}$ neurons (62 ± 9 nM) at the end of 2 h OGD.

In contrast, $[Ca^{2+}]_i$ rose at a rate of 4.4 nM/min in NHE1 $^{+/+}$ neurons during REOX and reached 325 ± 34 nM at 60 min REOX (Fig. 5*A*). Consistent with this finding, either HOE 642 or genetic ablation of NHE1 significantly attenuated the increase in $[Ca^{2+}]_i$ during REOX (Fig. 5*A*). $[Ca^{2+}]_i$ in NHE1 $^{+/+}$ neurons treated with HOE 642 after REOX was 104 ± 12 nM. NHE1 $^{-/-}$ neurons had 150 ± 10 nM $[Ca^{2+}]_i$ at 60 min REOX. HOE 642 also blocked Ca^{2+} changes in NHE1 $^{+/-}$ after OGD/REOX (86 ± 12 nM at 60 min REOX, compared with a control value of 325 ± 34 nM in

NHE1 $^{+/+}$ neurons). These findings suggest that NHE1 activity is required for intracellular Ca^{2+} rise in neurons after OGD.

The lack of $Ca^{2+}{}_i$ rise at the end of 2 h of OGD is in contrast to the study in mouse cortical neuron culture (Goldberg and Choi, 1993). We speculated that our current OGD treatment was mild and the induction of hypoxia was slow. Therefore, loss of ATP energy and Ca^{2+} homeostasis may develop slowly and moderately. The ATP level was ~12% of the control at the end of 2 h OGD (data not shown), determined by ATPlite (PerkinElmer, Boston, MA). Second, Ca^{2+} may be buffered by intracellular Ca^{2+} stores [endoplasmic reticulum (ER) and mitochondria]. Such a possibility has been revealed in our recent studies in astrocytes (Kintner et al., 2005). As shown in Figure 5, *B* and inset, a significant rise in $Ca^{2+}{}_i$ after OGD was unmasked when ER Ca^{2+}-ATPase was inhibited with thapsigargin. This OGD-mediated Ca^{2+} accumulation in ER was blocked by NHE1 inhibition.

Reversal of Na^+/Ca^{2+} exchange leads to the rise in $[Ca^{2+}]_i$ after OGD/REOX

We hypothesized that NHE1 activity contributes to the OGD/REOX-mediated Ca^{2+} rise by triggering a reversal of Na^+/Ca^{2+} exchange. To examine this possibility, we tested whether SEA0400, a potent inhibitor of the reverse mode of Na^+/Ca^{2+} exchange, could block the rise in intracellular Ca^{2+}. As shown in Figure 5*C*, in the presence of 1 μM SEA0400, OGD/REOX failed to elicit a time-dependent rise in $[Ca^{2+}]_i$, which was in contrast to the OGD/REOX-positive control neurons. This implies that activation of the reverse mode of the Na^+/Ca^{2+} exchanger causes a rise in $[Ca^{2+}]_i$ after OGD/REOX. OGD/REOX-mediated Ca^{2+} rise was abolished when both NHE1 and Na^+/Ca^{2+} exchange were inhibited. Most importantly, SEA0400 had no additional inhibition on Ca^{2+} changes in NHE1 $^{-/-}$ cells (Fig. 5*C*).

It has been suggested recently that NHE1 activation leads to mitochondrial Ca^{2+} overload in response to H_2O_2-mediated oxidative stress (Teshima et al., 2003). We therefore investigated whether stimulation of NHE1 activity after OGD/REOX affects mitochondrial Ca^{2+} loading in cortical neurons. NHE1 $^{+/+}$ neurons were exposed to 10 μM FCCP and 2.5 μg/ml oligomycin under Ca^{2+}-free conditions. There was no significant release of Ca^{2+} in response to FCCP/oligomycin in normoxic control neurons (peak value, 7 ± 13 nM) (Fig. 5*D*). This is consistent with the report by Brocard et al. (2001). After NHE1 $^{+/+}$ neurons were subjected to OGD/REOX, the peak of releasable Ca^{2+} from mitochondria was significantly increased (48 ± 5 nM) (Fig. 5*D*). Moreover, in NHE1 $^{-/-}$ neurons, a negligible level of mitochondrial free Ca^{2+} was released in response to FCCP/oligomycin (−2 ± 5 nM). After OGD/REOX, releasable free mitochondrial Ca^{2+} was only moderately increased (18 ± 2 nM) (Fig. 5*D*), and it was significantly lower than that in NHE1 $^{+/+}$ neurons (Fig. 5*D*).

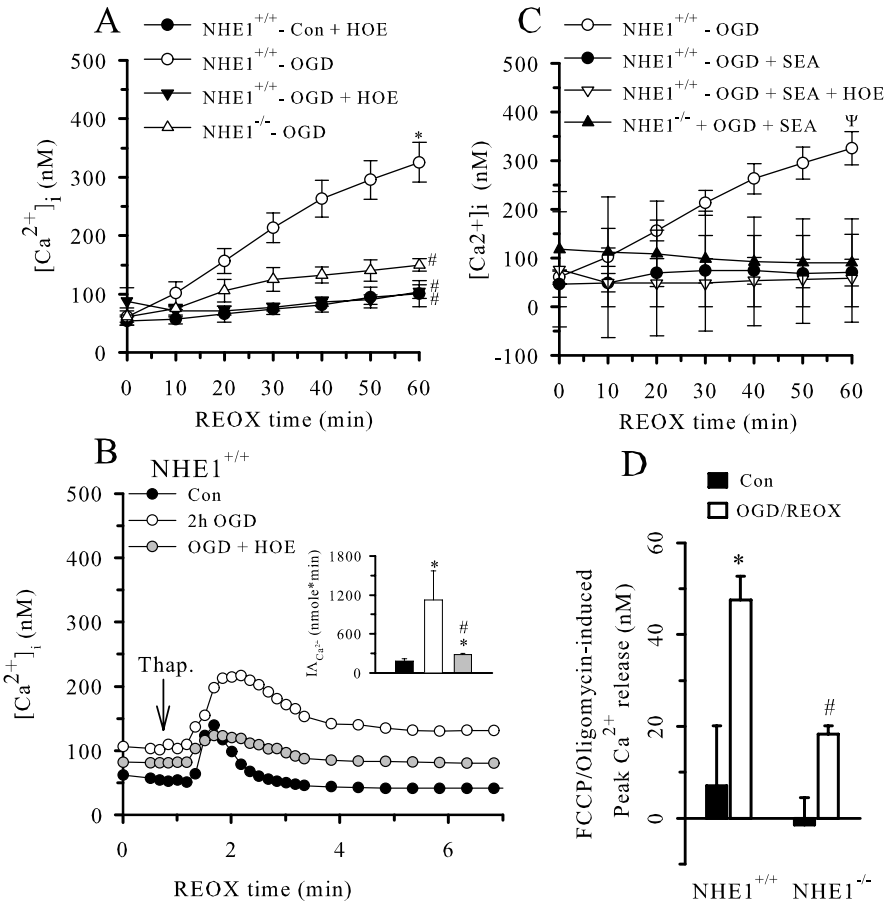

Figure 5. Ablation of NHE1 activity reduces OGD/REOX-induced increase in $[Ca^{2+}]_i$. ***A***, $[Ca^{2+}]_i$ was measured with fura-2 AM at the end of 2 h OGD and every 10 min over a 60 min period of REOX. Sister cultures were incubated for 3 h in normoxic control buffers. In HOE 642 treatment experiments, 1 μM HOE was present throughout the OGD and REOX periods. ***B***, Thapsigargin (Thap.; 1 μM)-induced Ca^{2+} release in the presence of 1.2 mM $[Ca^{2+}]_o$. Inset, Integrated area (IA) of Ca^{2+} release. ***C***, Neurons were treated with 1 μM SEA0400 or 1 μM SEA0400 plus 1 μM HOE 642 throughout the OGD/REOX period. ***D***, After OGD/REOX, NHE1 $^{+/+}$ or NHE1 $^{-/-}$ neurons were exposed to $[Ca^{2+}]_o$-free buffer containing 10 μM FCCP plus 2.5 μg/ml oligomycin for 4 min to stimulate release of Ca^{2+} from mitochondria. Data are means ± SE ($n = 4$–5). $^*p < 0.05$ versus NHE1 $^{+/+}$ Con; $^\#p < 0.001$ versus NHE1 $^{+/+}$ OGD/REOX; $^\Psi p < 0.001$ versus NHE1 $^{+/+}$ OGD/REOX plus SEA. Error bars represent SE.

Together, these results suggest that mitochondria sequester a small amount of Ca^{2+} in normoxic control neurons. OGD/REOX triggered a significantly greater accumulation of Ca^{2+} in mitochondria of NHE1 $^{+/+}$ neurons than of NHE1 $^{-/-}$ neurons.

Inhibition of NHE1 activity reduces OGD/REOX-mediated Cyt C release

Data in Figure 5 suggest that NHE1 activity plays a role in ischemic ER and mitochondrial stress. We therefore investigated whether mitochondrial Cyt C release, a hallmark of mitochondrial damage (Cao et al., 2004), is altered after OGD/REOX. In normoxic control NHE1 $^{+/+}$ neurons, Cyt C staining showed an abundant and punctated perinuclear expression pattern (Fig. 6*A*, left, arrows). Some punctated Cyt C staining, suggesting mitochondrial Cyt C expression, was also observed in neurites. Normal neuronal morphology was seen in the brightfield images (Fig. 6*A*, arrowheads, right top), and no PI-positive staining was found in these corresponding normoxic NHE1 $^{+/+}$ neurons (Fig. 6*A*, arrowheads, right bottom). In contrast, after 2 h OGD/22 h REOX, immunoreactivity for Cyt C was not detected in most of the NHE1 $^{+/+}$ neurons (Fig. 6*B*, left, arrows). These neurons exhibited swollen and degenerated morphology (arrowheads, right top) accompanied with positive staining for PI (Fig. 6*B*,

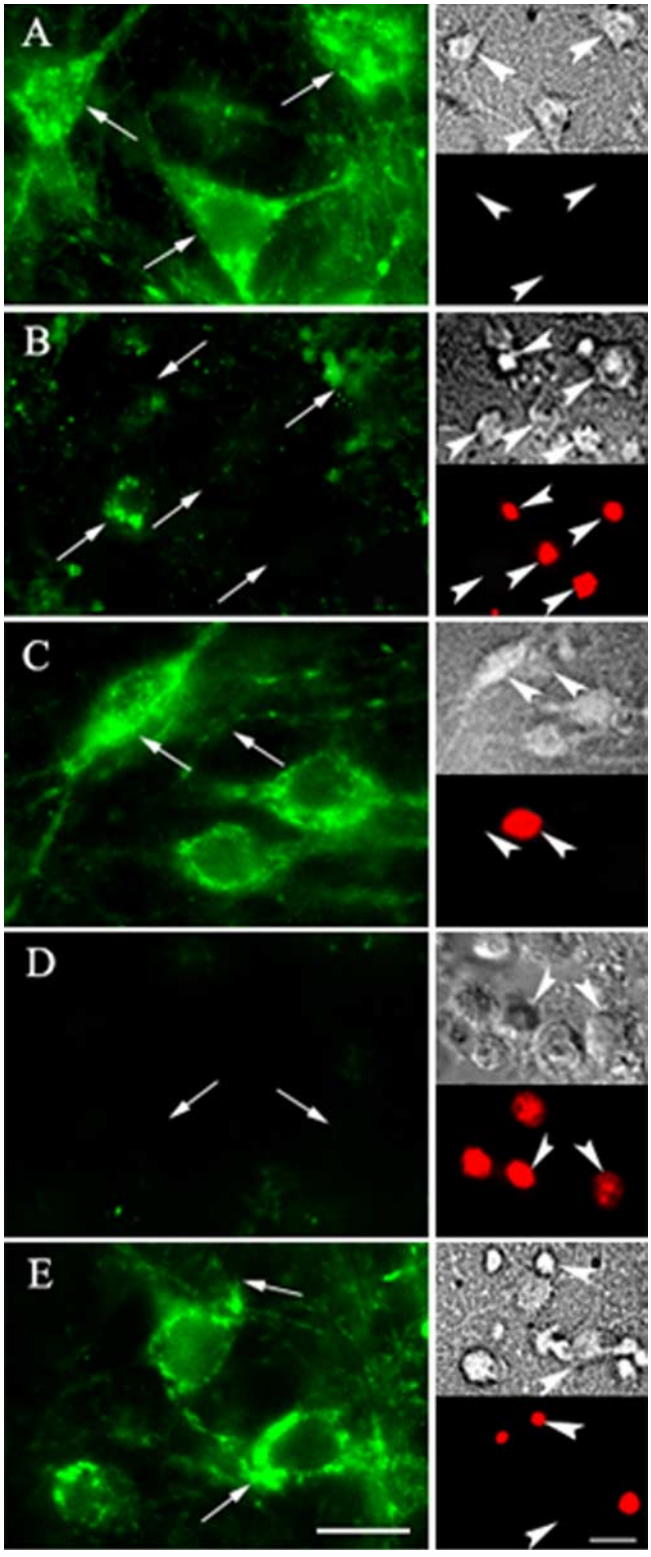

Figure 6. Inhibition of NHE1 activity reduces OGD/REOX-mediated cytochrome *c* release. The release of Cyt C in NHE1 $^{+/+}$ neurons was visualized by an anti-Cyt C antibody staining. Cell death was determined by PI staining. For HOE 642 treatment, NHE1 $^{+/+}$ neurons were incubated in EMEM in the presence of 1 μM HOE 642 at 37°C during 2–3 h of OGD and 21–22 h of REOX. Sister NHE1 $^{+/+}$ cultures were incubated for 24 h in normoxic control buffers. ***A***, Control buffers. ***B***, Two hours of OGD/22 h of REOX. ***C***, Two hours of OGD/22 h of REOX plus 1 μM HOE 642. ***D***, Three hours of OGD/21 h of REOX. ***E***, Three hours of OGD/21 h of REOX plus HOE 642. Left, Anti-Cyt C antibody staining. Right, top, Bright field. Right, bottom, PI staining. Arrows, Cyt C staining. Arrowheads, The cells corresponding to the Cyt C localization. Scale bar, 10 μm. Images shown are representative of four experiments.

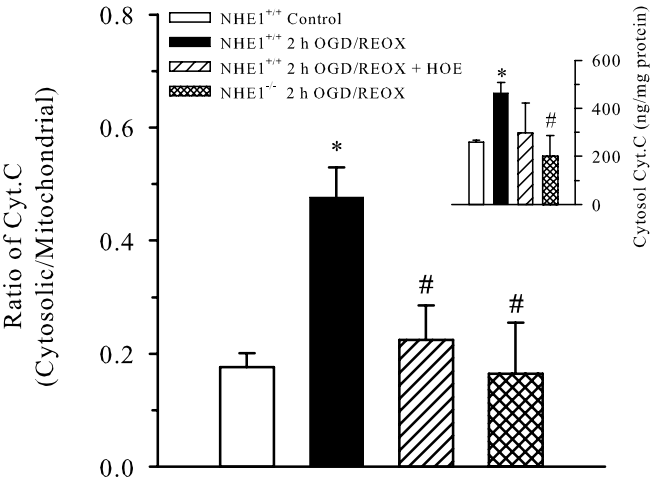

Figure 7. Quantification of Cyt C release after OGD/REOX. NHE1 $^{+/+}$, NHE1 $^{-/-}$, or NHE1 $^{+/+}$ neurons treated with 1 μM HOE 642 underwent 2 h of OGD and 22 h of REOX. Subcellular fractions (cytosolic vs mitochondrial) were prepared, and Cyt C content was assessed with a Quantikine M Rat/Mouse Cytochrome C Immunoassay kit. Inset, Cyt C in cytosolic fraction. Data are means ± SD ($n = 3$–4 cultures). *$p < 0.001$ versus NHE1 $^{+/+}$ Con; #$p < 0.05$ versus NHE1 $^{+/+}$ OGD/REOX. Error bars represent SD.

right bottom, arrowheads). The loss of Cyt C immunoreactive signals suggests that Cyt C was released from mitochondria and subsequently degraded after OGD/REOX. One neuron shown in the left center maintained some level of Cyt C expression and stained negative for PI. This again revealed a positive correlation between Cyt C release and cell death. However, when NHE1 activity was inhibited with 1 μM HOE 642, OGD-mediated Cyt C release was significantly attenuated. Figure 6*C* (left, arrows) illustrates that strong Cyt C immunoreactivity was preserved in the HOE 642-treated NHE1 $^{+/+}$ neurons. Brightfield images of these cells showed improved cellular morphology (Fig. 6*C*, right top). The NHE1 $^{+/+}$ neurons containing abundant Cyt C did not take up PI (Fig. 6*C*, right bottom, arrowheads). The PI-positive cell in the field shown expressed a diffused, reduced staining for Cyt C.

In addition, we also examined whether a similar Cyt C release profile was found at 3 h OGD/21 h REOX. Many cells lost Cyt C immunoreactive signals after 3 h OGD/21 h REOX (Fig. 6*D*, left, arrows). These cells concurrently took up PI (Fig. 6*D*, right bottom, arrowheads). In contrast, both Cyt C release and cell death were prevented in NHE1 $^{+/+}$ neurons treated with HOE 642 (Fig. 6*E*, left and right, arrows). These findings further suggest that NHE1 activity plays a role in ischemic mitochondrial damage.

To further quantify Cyt C release, we determined Cyt C content from cytosolic and mitochondrial fractions of neurons with a Cyt C immunoassay. As shown in Figure 7 (inset), under normoxic conditions, the Cyt C content of the cytosol was low, and most of the Cyt C resided in the mitochondria of NHE1 $^{+/+}$ neurons. However, OGD/REOX led to ~100% increase in cytosolic Cyt C. The ratio of Cyt C content in the cytosol versus mitochondria was increased in a similar manner (Fig. 7). Either inhibition of NHE1 activity with 1 μM HOE 642 or genetic ablation of NHE1 activity abolished the loss of Cyt C from mitochondria. Together, these findings are consistent with the immunostaining data. These experiments demonstrated that inhibition of NHE1 activity significantly protects mitochondrial integrity in neurons after OGD/REOX. However, it is unknown whether intrinsic property of mitochondria is altered in NHE1 $^{-/-}$ neurons. In light of a reduced mitochondrial Ca^{2+} accumulation in NHE1 $^{-/-}$ neu-

Table 1. Physiological parameters in NHE1$^{+/+}$ control and HOE 642-treated NHE1$^{+/+}$ mice

	Sham ($n = 3$)	Control NHE1$^{+/+}$ mice ($n = 4$)		HOE 642-treated NHE1$^{+/+}$ mice ($n = 4$)	
		Preischemia	Ischemia	Preischemia	Ischemia
MABP (mmHg)	84.7 ± 12.7	85.1 ± 8.9	83.0 ± 5.1	83.6 ± 6.6	81.0 ± 6.7
pH	7.36 ± 0.08	7.34 ± 0.07	7.42 ± 0.10	7.33 ± 0.04	7.41 ± 0.07
P_aCO_2 (mmHg)	35.4 ± 1.4	44.0 ± 12.4	32.5 ± 10.8	40.6 ± 8.0	32.5 ± 5.5
P_aO_2 (mmHg)	119.3 ± 56.3	132.0 ± 51.5	110.0 ± 38.5	125.5 ± 45.1	136.5 ± 59.2
Na^+ (mM)	146.0 ± 1.7	145.5 ± 0.6	144.5 ± 1.3	145.8 ± 4.8	143.8 ± 4.7
K^+ (mM)	4.7 ± 0.9	4.3 ± 0.7	5.6 ± 0.4*	3.8 ± 0.7	5.1 ± 0.8*
CBF (%; $n = 4–9$)	100	100	13.0 ± 6.3	100	10.0 ± 8.7
Rectal temperature (°C)	36.9 ± 0.1	37.0 ± 0.2	37.0 ± 0.2	37.0 ± 0.1	36.8 ± 0.3

Values are expressed as mean ± SD. MABP, Mean arterial blood pressure before blood sampling.

*$p < 0.05$ versus preischemia.

Table 2. Tympanic membrane temperature in NHE1$^{+/+}$ control and HOE 642-treated NHE1$^{+/+}$ mice

	Control NHE1$^{+/+}$ mice		HOE 642-treated NHE1$^{+/+}$ mice	
Temprature (°C)	Contralateral	Ipsilateral	Contralateral	Ipsilateral
Before MCAO (15 min)	36.8 ± 0.07	36.7 ± 0.07	36.8 ± 0.00	36.9 ± 0.23
During MCAO (60 min)	36.9 ± 0.14	36.0 ± 0.07	36.7 ± 0.07	36.0 ± 0.28
During MCAO (60–120 min)	36.5 ± 0.64	35.8 ± 0.49	36.0 ± 0.57	35.5 ± 0.71

Values are expressed as mean ± SD. $n = 2$.

rons under normoxic control conditions (Fig. 5*D*), additional study is needed to clarify this issue.

HOE 642 has no effects on physiological parameters before and after ischemia in mice

We next investigated whether inhibition of NHE1 activity is neuroprotective in cerebral focal ischemia. Mean arterial blood pressure, pH, P_aCO_2, P_aO_2, Na^+, and K^+ were not significantly different between sham, nontreated, and HOE 642-treated NHE1$^{+/+}$ mice under control conditions (Table 1). After 1 h of MCAO, the physiological measurements remained unchanged in either NHE1$^{+/+}$ control or HOE 642-treated NHE1$^{+/+}$ mice. Plasma Na^+ concentrations after ischemia were the same in either NHE1$^{+/+}$ control or HOE 642-treated NHE1$^{+/+}$ mice. However, in both groups, plasma K^+ concentrations significantly increased after ischemia ($p < 0.05$). This increase may reflect the release of intracellular K^+ as a result of surgery-induced tissue damage, as the sham-surgery animals also showed an increase in plasma K^+ (4.7 ± 0.9 mM).

NHE1$^{+/+}$ control or HOE 642-treated mice showed a similar degree of decrease in regional CBF after MCAO induction (13.0 ± 6.3 vs 10.0 ± 8.7%) (Table 1). These differences in CBF changes were not statistically significant ($p > 0.05$). MCAO caused a ~0.7–0.9°C reduction in ipsilateral tympanic membrane temperature compared with contralateral side, which persisted at 1–2 h reperfusion (Table 2). This drop in temperature occurred in both NHE1$^{+/+}$ control and HOE 642-treated NHE1$^{+/+}$ mice as well as NHE1$^{+/-}$ mice (36.4°C at 1 h reperfusion). Therefore, neuroprotective effects observed in HOE 642-treated NHE1$^{+/+}$ mice and NHE1$^{+/-}$ mice unlikely result from mild hypothermia after MCAO.

Inhibition of NHE1 with HOE 642 is neuroprotective in focal ischemia

We first examined whether inhibition of NHE1 activity with HOE 642 is neuroprotective in the focal ischemia model. Infarction volume was assessed in control- and HOE 642-treated NHE1$^{+/+}$ brains (Fig. 8*A*). The predominant lesion was found in a region 4–6 mm posterior to the frontal pole, where blood supply is primarily from the middle cerebral artery. After 2 h of MCAO and 24 h of reperfusion, the average total infarction volume (cortical plus subcortical areas) in control NHE1$^{+/+}$ mice was 84.8 ± 17.7 mm^3 (Fig. 8*B*). In HOE 642-treated NHE1$^{+/+}$ mice, the average total infarct volume was 56.8 ± 25.9 mm^3 ($p < 0.05$).

We then tested whether inhibition of NHE1 activity reduces edema. Water content in control and HOE 642-treated NHE1$^{+/+}$ mice were shown in Figure 8*C*. In control NHE1$^{+/+}$ mice, water content averaged 78.5% in the contralateral hemispheres. Ischemia led to a significant increase in water content in the ipsilateral hemispheres of control NHE1$^{+/+}$ mice (82.2%; $p < 0.01$) (Fig. 8*C*). In HOE 642-treated NHE1$^{+/+}$ mice, the increase in water content was less than that in control NHE1$^{+/+}$ mice, but it remained significantly higher than that in contralateral sides (78.8 ± 0.3 vs 80.7 ± 2.3%; $p < 0.05$) (Fig. 8*C*).

A decrease in infarct size in NHE1$^{+/-}$ mice after focal ischemia

Expression of NHE1 protein in NHE1$^{+/+}$, NHE1$^{+/-}$, and NHE1$^{-/-}$ mice was determined using a specific anti-NHE1 polyclonal antibody. As shown in Figure 9*A*, a strong NHE1 band at a molecular weight of ~110 K_D was recognized in NHE1$^{+/+}$ cortex. In contrast, no NHE1 expression was detected in NHE1$^{-/-}$ cortex. However, expression of NHE1 protein was decreased ~70% in NHE1$^{+/-}$ mice ($p < 0.05$) (Fig. 9*A*). A similar level of βIII-tubulin was detected in the same blot of three genotypes.

NHE1$^{-/-}$ mice cannot be used in this *in vivo* study of focal ischemia because of the high mortality and seizure disorder in these animals (Cox et al., 1997; Bell et al., 1999). Because NHE1$^{+/-}$ mice exhibited a significant reduction of NHE1 protein in the cortex, we investigated whether this reduced expression would provide some degree of neuronal protection. NHE1$^{+/+}$ and NHE1$^{+/-}$ mice underwent 2 h of MCAO and 24 h of reperfusion. Infarction volume was assessed in NHE1$^{+/+}$ and NHE1$^{+/-}$ brains. The predominant lesion was found in a region 4–6 mm posterior to the frontal pole (Fig. 9*B*). After 2 h of MCAO and 24 h of reperfusion, the average total infarction volume in NHE1$^{+/+}$ mice was 85.4 ± 4.8 mm^3. In NHE1$^{+/-}$ mice, the average total infarct volume was 58.2 ± 11.8 mm^3 ($p < 0.05$). This further confirms that NHE1 activity plays a role in focal cerebral ischemic damage.

Water content was also measured in NHE1$^{+/+}$ and NHE1$^{+/-}$ mice after focal ischemia, as shown in Figure 9*D*. After ischemia, the water content in ipsilateral hemispheres of NHE1$^{+/+}$ mice showed a significant increase (78.8 vs 82.7%; $p < 0.01$) (Fig. 9*D*). In NHE1$^{+/-}$ mice, water content was also significantly increased in the ipsilateral sides (78.6 ± 2.1 vs 81.3 ± 0.4%; $p < 0.01$). Thus,

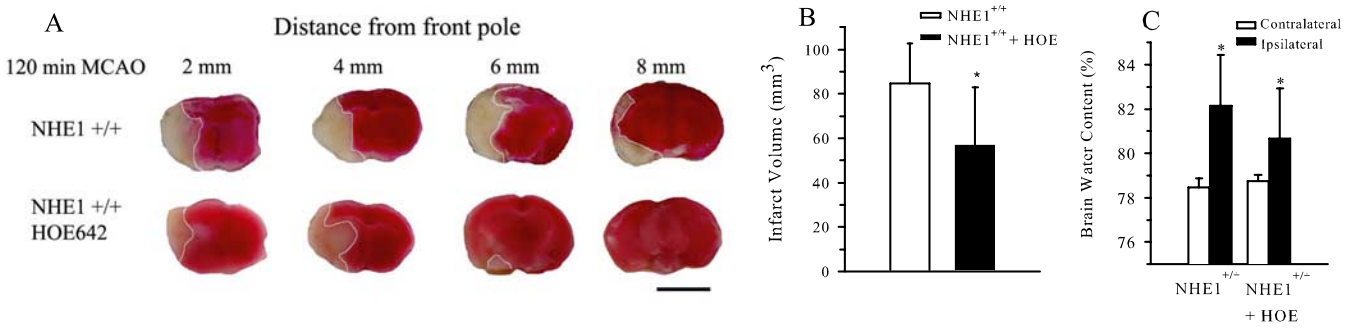

Figure 8. Inhibition of NHE1 activity with HOE 642 reduces infarction after focal ischemia. ***A***, ***B***, After 2 h of MCAO and 24 h of reperfusion, saline-treated control and HOE 642-treated NHE1 $^{+/+}$ mice were killed (see Materials and Methods). Infarction volume (outlined area) was determined by TTC staining. Data are means ± SD ($n = 4–6$). *$p < 0.05$ versus NHE1 $^{+/+}$. Scale bar, 5 mm. ***C***, Focal ischemia induced a significant increase in water content. *$p < 0.01$ versus contralateral. Error bars represent SD.

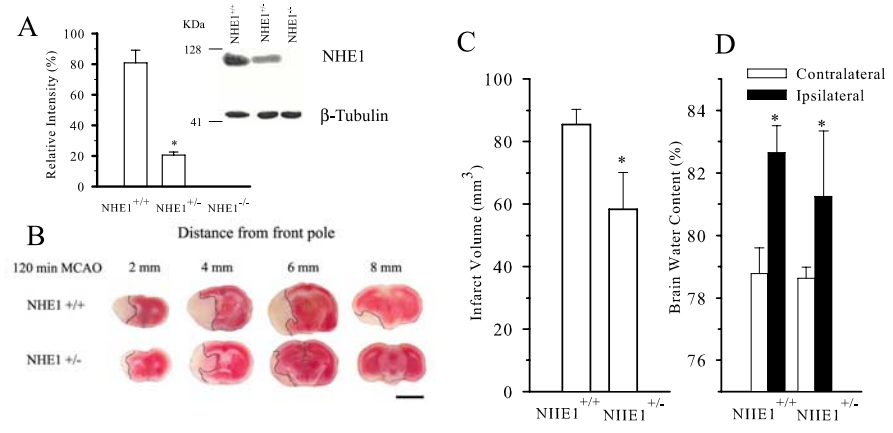

Figure 9. Less infarct formation in NHE1 $^{+/-}$ mice after focal ischemia. ***A***, Crude cortex membrane proteins of three genotypes were separated electrophoretically as described in Materials and Methods. Expression of NHE1 and β-tubulin III in NHE1 $^{+/+}$, NHE1 $^{+/-}$, and NHE1 $^{-/-}$ mouse cortex is shown on the same blot. Densitometric analysis of immunoblots is presented as a ratio of NHE1/β-tubulin III band intensity. Data are means ± SD ($n = 3–5$). ***B***, ***C***, After 2 h MCAO and 24 h reperfusion, infarction volume in NHE1 $^{+/+}$ or NHE1 $^{+/-}$ mice was determined by TTC staining. *$p < 0.05$ versus NHE1 $^{+/+}$. Data are means ± SD ($n = 4$). Scale bar, 5 mm. ***D***, Water content in NHE1 $^{+/+}$ and NHE1 $^{+/-}$ mice after 2 h of MCAO and 24 h of reperfusion. Data are means ± SD ($n = 4–6$). *$p < 0.01$ versus contralateral. Error bars represent SD.

reduction of NHE1 protein in NHE1 $^{+/-}$ mice did not significantly improve cerebral edema.

Discussion

The role of NHE1 in steady-state pH_i of cortical neurons

In response to NH_3/NH_4-mediated acidosis, cortical neurons quickly extruded H^+ in a process primarily mediated by NHE1 activity. Inhibition of NHE1 activity with HOE 642 blocked ~92% of the initial pH recovery rate in NHE1 $^{+/+}$ cortical neurons. NHE1 $^{-/-}$ neurons also failed to regulate pH_i after acidosis. The consistent responses in HOE 642-treated cells and NHE1 $^{-/-}$ neurons imply that HOE 642 (1.0 μM) targets only NHE1. HOE 642 is a potent, highly selective NHE1 inhibitor with an IC_{50} value of 0.08 μM for NHE1 (Scholz et al., 1995). In contrast, the IC_{50} values of HOE 642 for NHE2, NHE3, and NHE4 are 1.6, 1000, and 250 μM, respectively (Scholz et al., 1995). The IC_{50} value of another HOE 642 analog, HOE 694, for NHE5 is 9.1 μM (Numata and Orlowski, 2001). If NHE2, NHE3, or NHE4 were involved in pH_i regulation in cortical neurons, then an effect on pH_i would have been observed in the presence of 1.0 μM HOE 642. Compared with NHE1, these plasma membrane isoforms are expressed in the rat cerebral cortex at significantly lower levels (Douglas et al., 2001). Our study provides functional evidence for an essential role of NHE1 in the regulation of pH_i in cortical neurons in the absence of HCO_3^-.

Inhibition of NHE1 activity is neuroprotective after both *in vitro* and *in vivo* ischemia

Stimulation of NHE1 activity is detrimental to the ischemic myocardium (Avkiran, 2001), and we recently reported that both pharmacological inhibition and genetic ablation of NHE1 reduced the impairment of Na^+ and Ca^{2+} homeostasis in cortical astrocytes after OGD (Kintner et al., 2004, 2005). In this study, we found that the selective NHE1 inhibitor HOE 642 significantly reduced OGD-mediated neuronal cell death by ~50% in NHE1 $^{+/+}$ mice. Genetic ablation of NHE1 attenuated neuronal cell death by ~37%. Moreover, a significant reduction in infarction in cerebral focal ischemia occurred when NHE1 activity was inhibited with HOE 642 in NHE1 $^{+/+}$ mice or in NHE1 knockdown (NHE1 $^{+/-}$) mice. This neuroprotection may result from a blockage of NHE1 activity in both astrocytes and neurons.

In this study, we took both pharmacological and genetic ablation approaches to elucidate the role of NHE1 in neuronal ischemic damage. The combination of these approaches overcame the shortcomings of each method. For instance, the spontaneous NHE1 mutant mice (slow-wave epilepsy) exhibit upregulation of NHE3 in cerebellum, Na^+ channel current density in hippocampal and cortical neurons, and downregulation of brain-specific anion exchanger isoform 3 in the hippocampus (Xia et al., 2003; Xue et al., 2003). In addition, NHE1-deficient brains exhibited regionally specific downregulation of many genes, implying that NHE1 may function as a signaling molecule (Zhou et al., 2004). In contrast, high concentrations of HOE 642 can affect multiple isoforms of NHE. Therefore, we were careful in the experimental design to avoid any potential nonspecific effects of HOE 642 by using a low concentration. By comparing the effects of inhibition of NHE1 with HOE 642 and genetic ablation of NHE1, we are able to rule out any compensatory effects from other genes in NHE1 null neurons. Additionally, we confirmed neuroprotection mediated by NHE1 knockdown using NHE1 heterozygous neurons or mice. All of these approaches gave similar results, and

we conclude that NHE1 indeed plays a role in disruption of Na^+ and Ca^{2+} homeostasis and neuronal damage after ischemia.

Inhibition of NHE1 activity fails to reduce ischemic edema formation

In the present study, knockdown of NHE1 expression or inhibition of NHE1 activity with HOE 642 was neuroprotective but did not reduce edema after transient focal ischemia. This finding implies that NHE1-mediated changes in Ca^{2+} overload and mitochondrial dysfunction may play a dominant role in ischemic cell death. In contrast, cell swelling associated with Na^+ entry via NHE1 is not critical in triggering the ischemic cell death. These noncorrelated effects between cell death and edema were also found with the NHE inhibitor SM20220. It was shown that although SM20220 (0.3 mg/kg) significantly reduced brain edema at 4 h reperfusion after 2 h MCAO in rats, it failed to reduce the infarction (Kuribayashi et al., 1999). However, continuous administration of SM20220 during reperfusion concurrently improved ischemic infarct formation, brain edema, and neutrophil accumulation (Suzuki et al., 2002). The edema formation at 24 h reperfusion in focal ischemia likely represents both cellular and vasogenic edema. This suggests that it may require inhibition of multiple NHE isoforms and/or in multiple cell types (neuron, glia, cerebral microvessel cells, and microphages) to suppress edema formation. However, in the current study, reduction of NHE1 activity alone may not be sufficient to target multiple pathways.

Stimulation of NHE1 activity triggers reverse-mode operation of Na^+/Ca^{2+} exchange

We further investigated the underlying mechanisms for this neuroprotection provided by NHE1 inhibition. Inhibition of NHE1 activity may protect neurons by reducing Na^+ loading, which is known to have deleterious effects on neurons (Stys, 2005). Second, blocking of the function of NHE1 in pH_i regulation may create a mild acidosis that may inhibit toxic pathways that are sensitive to pH_i (Tombaugh and Sapolsky, 1993). In addition, inhibition of NHE1 activity can prevent intracellular Na^+ and Ca^{2+} overload and reduce the Ca^{2+}-mediated cascade of deleterious events. We found that REOX triggered an approximately sevenfold increase in $[Na^+]_i$ in NHE1$^{+/+}$ neurons. HOE 642 and genetic ablation of NHE1 activity blocked Na^+ accumulation by ~50%. The remaining Na^+ loading (NHE1-insensitive) may be the result of a reduction in Na^+ extrusion by Na^+/K^+ ATPase (intracellular ATP level was ~40% of the control at 1 h REOX; data not shown) and stimulation of other Na^+ entry pathways including the Na^+ channel. Sheldon et al. (2004) recently reported that in addition to NHEs, reversal of Na^+/Ca^{2+} exchange and a Gd^{3+}-sensitive pathway also contribute to Na^+ influx in rat hippocampal neurons during and immediately after chemical anoxia.

In addition to an impairment of intracellular Na^+ homeostasis, $[Ca^{2+}]_i$ was increased by 1.5-fold during REOX after OGD. This Ca^{2+} overload was abolished by pharmacological inhibition or genetic ablation of NHE1 activity. We believe that NHE1-mediated disruption of intracellular Na^+ homeostasis subsequently triggered Ca^{2+} entry via the reverse-mode operation of Na^+/Ca^{2+} exchange.

To date, the function of NHE1 in conjunction with reversal of the Na^+/Ca^{2+} exchange system has not been established in neurons. Our recent thermodynamic analysis revealed that reverse-mode operation of Na^+/Ca^{2+} exchange can occur when $[Na^+]_i$ increases >25 mM in astrocytes (Kintner et al., 2005). Such a mechanism is also involved in astrocyte death after hypoxia (Bondarenko et al., 2005). Using our experimentally determined ion concentrations in neurons, the Na^+/Ca^{2+} exchange system is predicted to function in the reverse mode when $[Na^+]_i$ increases to ~13 mM at a plasma membrane potential of −70 mV. After OGD/REOX, $[Na^+]_i$ in NHE1$^{+/+}$ neurons increased to ~40 mM. The plasma membrane potential in these cells was depolarized by ~30% after OGD [evaluated by the DiBAC4(3) fluorescence-imaging technique; data not shown]. These changes would strongly favor an inwardly directed Ca^{2+} current via the Na^+/Ca^{2+} exchange. The following data further support the correlation between NHE1 and Na^+/Ca^{2+} exchange: (1) both $[Na^+]_i$ and $[Ca^{2+}]_i$ were increased during REOX; (2) the increases in $[Na^+]_i$ and $[Ca^{2+}]_i$ were both partially sensitive to NHE1 inhibition; and (3) the OGD/REOX-mediated $[Ca^{2+}]_i$ increase was attenuated by SEA0400. SEA0400 is a potent but nonspecific inhibitor of Na^+/Ca^{2+} exchange that also suppresses other non-Na^+/Ca^{2+} exchanger-mediated Ca^{2+} currents (Reuter et al., 2002). Together, these data lead us to conclude that stimulation of NHE1 activity in cortical neurons causes intracellular Na^+ overload and subsequently triggers Ca^{2+} influx via the reverse mode of Na^+/Ca^{2+} exchange.

It has been reported that reversal of Na^+/Ca^{2+} exchange is an important contributor to the early increase in $[Ca^{2+}]_i$ caused by NMDA and non-NMDA receptor activation in rat cortical neurons (Hoyt et al., 1998a). However, inhibition of the reverse mode of Na^+/Ca^{2+} exchange with KB-R7943 does not reduce the prolonged Ca^{2+} load nor neuronal cell death induced by glutamate receptor activation (Hoyt et al., 1998a). In rat cerebellar granule cells, a large part of NMDA-induced Ca^{2+}influx in depolarized and glucose-deprived cells is mediated by reverse Na^+/Ca^{2+} exchange. This high level of reverse Na^+/Ca^{2+} exchange is maintained by a sustained Na^+ influx via NMDA channels and depolarization of the plasma membrane under conditions of glucose deprivation (Czyz and Kiedrowski, 2002). In neurons energized by glucose, however, most Ca^{2+} enters directly via NMDA channels, and Na^+/K^+ ATPase regenerates Na^+ and K^+ concentration gradients, which prevents Na^+/Ca^{2+} exchange reversal (Czyz and Kiedrowski, 2002). These findings are consistent with ours in that NHE1-mediated intracellular Na^+ accumulation after OGD/REOX is a prerequisite for reversal of Na^+/Ca^{2+} exchange and Ca^{2+} overload. It has also been reported that Na^+ entry and Na^+/Ca^{2+} exchange play a role in anoxic white matter injury (Stys, 2004).

The role of NHE1 activity in ischemic mitochondrial damage

Mitochondrial Ca^{2+} overload is a major trigger of the mitochondrial death pathway, which features the loss of mitochondrial membrane potential, the opening of the mitochondrial permeability transition pore, release of Cyt C, and enhanced generation of reactive oxygen species (Hoyt et al., 1998b; Brookes et al., 2004; Cao et al., 2004). Inhibition of NHE1 activity remarkably suppressed cytosolic Na^+ and Ca^{2+} accumulation and mitochondrial Ca^{2+} overload in cardiomyocytes after H_2O_2-induced oxidative stress (Teshima et al., 2003). HOE 642 also reduced caspase-3 activity and annexin V fluorescence in cardiomyocytes stimulated by H_2O_2 (Teshima et al., 2003). This suggests that NHE1 function not only affects cytosolic Na^+ and Ca^{2+} homeostasis, but it also alters mitochondrial Ca^{2+} homeostasis and functions. In the current study, we found that OGD/REOX caused a significant increase in mitochondrial Ca^{2+} accumulation and Cyt C release. However, this increase in mitochondrial Ca^{2+} overload was attenuated in NHE1$^{-/-}$ neurons. Inhibition

of NHE1 activity with HOE 642 prevented the OGD/REOX-mediated Cyt C release and death of NHE1$^{+/+}$ neurons. Together, our findings support the view that NHE1 activity plays a role in mitochondrial dysfunction in oxidative cell damage. Therefore, preserving mitochondrial integrity by NHE1 inhibition may in part contribute to the neuroprotection in both *in vitro* and *in vivo* ischemia models.

In addition to targeting plasma membrane NHEs, recent reports suggest that NHE inhibitors could exert their anti-ischemic effect at the mitochondrial level. HOE 642 (7 μM) delayed mitochondrial matrix acidification and slowed ATP depletion in cardiomyocytes during ischemic conditions despite enhanced mitochondrial Ca^{2+} accumulation (Ruiz-Meana et al., 2003). The NHE inhibitor SM20550 attenuated Ca^{2+} overload in rat myocardial mitochondria after ischemia and reperfusion (Yamamoto et al., 2002). It remains to be further clarified whether the HOE 642 (1 μM)-mediated neuroprotection in the current study results from targeting of both cytoplasmatic NHE1 and mitochondrial NHEs or whether NHE1$^{-/-}$ neurons exhibit altered mitochondrial Ca^{2+} buffering activity.

In summary, we report here that NHE1 activity contributes to ischemic neuronal death after *in vitro* and *in vivo* ischemia. The underlying mechanisms include the activation of NHE1 activity in conjunction with the Na^+/Ca^{2+} exchanger leading to disruption of intracellular Na^+ and Ca^{2+} homeostasis. In addition to cytosolic Ca^{2+} overload, NHE1 activity also plays a detrimental role in mitochondrial Ca^{2+} overload and mitochondrial dysfunction after ischemia.

References

Avkiran M (2001) Protection of the ischaemic myocardium by Na^+/H^+ exchange inhibitors: potential mechanisms of action. Basic Res Cardiol 96:306–311.

Baumgartner M, Patel H, Barber DL (2004) Na^+/H^+ exchanger NHE1 as plasma membrane scaffold in the assembly of signaling complexes. Am J Physiol Cell Physiol 287:C844–C850.

Beck J, Lenart B, Kintner DB, Sun D (2003) Na-K-Cl cotransporter contributes to glutamate-mediated excitotoxicity. J Neurosci 23:5061–5068.

Bell SM, Schreiner CM, Schultheis PJ, Miller ML, Evans RL, Vorhees CV, Shull GE, Scott WJ (1999) Targeted disruption of the murine Nhe1 locus induces ataxia, growth retardation, and seizures. Am J Physiol 276:C788–C795.

Bondarenko A, Svichar N, Chesler M (2005) Role of Na^+-H^+ and Na^+-Ca^{2+} exchange in hypoxia-related acute astrocyte death. Glia 49:143–152.

Boyarsky G, Ransom B, Schlue WR, Davis MB, Boron WF (1993) Intracellular pH regulation in single cultured astrocytes from rat forebrain. Glia 8:241–248.

Brett CL, Donowitz M, Rao R (2005) Evolutionary origins of eukaryotic sodium/proton exchangers. Am J Physiol Cell Physiol 288:C223–C239.

Brocard JB, Tassetto M, Reynolds IJ (2001) Quantitative evaluation of mitochondrial calcium content in rat cortical neurones following a glutamate stimulus. J Physiol (Lond) 531:793–805.

Brookes PS, Yoon Y, Robotham JL, Anders MW, Sheu SS (2004) Calcium, ATP, and ROS: a mitochondrial love-hate triangle. Am J Physiol Cell Physiol 287:C817–C833.

Cao G, Xiao M, Sun F, Xiao X, Pei W, Li J, Graham SH, Simon RP, Chen J (2004) Cloning of a novel Apaf-1-interacting protein: a potent suppressor of apoptosis and ischemic neuronal cell death. J Neurosci 24:6189–6201.

Ch'en FF, Dilworth E, Swietach P, Goddard RS, Vaughan-Jones RD (2003) Temperature dependence of Na^+-H^+ exchange, Na^+-HCO3-cotransport, intracellular buffering and intracellular pH in guinea-pig ventricular myocytes. J Physiol (Lond) 552:715–726.

Chen H, Luo J, Kintner DB, Shull GE, Sun D (2005) Na^+-dependent chloride transporter (NKCC1)-null mice exhibit less gray and white matter damage after focal cerebral ischemia. J Cereb Blood Flow Metab 25:54–66.

Choi DW (1995) Calcium: still center-stage in hypoxic-ischemic neuronal death. Trends Neurosci 18:58–60.

Cox GA, Lutz CM, Yang CL, Biemesderfer D, Bronson RT, Fu A, Aronson PS, Noebels JL, Frankel WN (1997) Sodium/hydrogen exchanger gene defect in slow-wave epilepsy mutant mice. Cell 91:139–148.

Czyz A, Kiedrowski L (2002) In depolarized and glucose-deprived neurons, Na^+ influx reverses plasmalemmal K^+-dependent and K^+-independent Na^+/Ca^{2+} exchangers and contributes to NMDA excitotoxicity. J Neurochem 83:1321–1328.

Denker SP, Huang DC, Orlowski J, Furthmayr H, Barber DL (2000) Direct binding of the Na-H exchanger NHE1 to ERM proteins regulates the cortical cytoskeleton and cell shape independently of H^+ translocation. Mol Cell 6:1425–1436.

Dent EW, Callaway JL, Szebenyi G, Baas PW, Kalil K (1999) Reorganization and movement of microtubules in axonal growth cones and developing interstitial branches. J Neurosci 19:8894–8908.

Douglas RM, Schmitt BM, Xia Y, Bevensee MO, Biemesderfer D, Boron WF, Haddad GG (2001) Sodium-hydrogen exchangers and sodium-bicarbonate co-transporters: ontogeny of protein expression in the rat brain. Neuroscience 102:217–228.

Goldberg MP, Choi DW (1993) Combined oxygen and glucose deprivation in cortical cell culture: calcium-dependent and calcium-independent mechanisms of neuronal injury. J Neurosci 13:3510–3524.

Goyal S, Mentone S, Aronson PS (2005) Immunolocalization of NHE8 in rat kidney. Am J Physiol Renal Physiol 288:F530–F538.

Hoyt KR, Arden SR, Aizenman E, Reynolds IJ (1998a) Reverse Na^+/Ca^{2+} exchange contributes to glutamate-induced intracellular Ca^{2+} concentration increases in cultured rat forebrain neurons. Mol Pharmacol 53:742–749.

Hoyt KR, Stout AK, Cardman JM, Reynolds IJ (1998b) The role of intracellular Na^+ and mitochondria in buffering of kainate-induced intracellular free Ca^{2+} changes in rat forebrain neurones. J Physiol (Lond) 509:103–116.

Kelly MP, Quinn PA, Davies JE, Ng LL (1997) Activity and expression of Na^+-H^+ exchanger isoforms 1 and 3 in kidney proximal tubules of hypertensive rats. Circ Res 80:853–860.

Kintner DB, Su G, Lenart B, Ballard AJ, Meyer JW, Ng LL, Shull GE, Sun D (2004) Increased tolerance to oxygen and glucose deprivation in astrocytes from Na^+/H^+ exchanger isoform 1 null mice. Am J Physiol Cell Physiol 287:C12–C21.

Kintner DB, Look A, Shull GE, Sun D (2005) Stimulation of astrocyte Na^+/H^+ exchange activity in response to in vitro ischemia in part depends on activation of extracellular signal-regulatory kinase. Am J Physiol Cell Physiol 289:C934–C945.

Kraus RL, Pasieczny R, Lariosa-Willingham K, Turner MS, Jiang A, Trauger JW (2005) Antioxidant properties of minocycline: neuroprotection in an oxidative stress assay and direct radical-scavenging activity. J Neurochem 94:819–827.

Kuribayashi Y, Itoh N, Kitano M, Ohashi N (1999) Cerebroprotective properties of SM-20220, a potent Na^+/H^+ exchange inhibitor, in transient cerebral ischemia in rats. Eur J Pharmacol 383:163–168.

Lenart B, Kintner DB, Shull GE, Sun D (2004) Na-K-Cl cotransporter-mediated intracellular Na^+ accumulation affects Ca^{2+} signaling in astrocytes in an *in vitro* ischemic model. J Neurosci 24:9585–9597.

Ma E, Haddad GG (1997) Expression and localization of Na^+/H^+ exchangers in rat central nervous system. Neuroscience 79:591–603.

Mellergard P, Ouyang YB, Siesjo BK (1993) Intracellular pH regulation in cultured rat astrocytes in CO_2 /HCO_3^- containing media. Exp Brain Res 95:371–380.

Numata M, Orlowski J (2001) Molecular cloning and characterization of a novel (Na^+,K^+)/H^+ exchanger localized to the trans-Golgi network. J Biol Chem 276:17387–17394.

Orlowski J, Grinstein S (2004) Diversity of the mammalian sodium/proton exchanger SLC9 gene family. Pflügers Arch 447:549–565.

Pei W, Liou AK, Chen J (2003) Two caspase-mediated apoptotic pathways induced by rotenone toxicity in cortical neuronal cells. FASEB J 17:520–522.

Phillis JW, Estevez AY, Guyot LL, O'Regan MH (1999) 5-(*N*-ethyl-*N*-isopropyl)-amiloride, an Na^+-H^+ exchange inhibitor, protects gerbil hippocampal neurons from ischemic injury. Brain Res 839:199–202.

Reuter H, Henderson SA, Han T, Matsuda T, Baba A, Ross RS, Goldhaber JI, Philipson KD (2002) Knockout mice for pharmacological screening:

testing the specificity of Na^+-Ca^{2+} exchange inhibitors. Circ Res 91:90–92.

Ruiz-Meana M, Garcia-Dorado D, Pina P, Inserte J, Agullo L, Soler-Soler J (2003) Cariporide preserves mitochondrial proton gradient and delays ATP depletion in cardiomyocytes during ischemic conditions. Am J Physiol Heart Circ Physiol 285:H999–H1006.

Scholz W, Albus U, Counillon L, Gogelein H, Lang HJ, Linz W, Weichert A, Scholkens BA (1995) Protective effects of HOE-642, a selective sodium-hydrogen exchange subtype 1 inhibitor, on cardiac ischaemia and reperfusion. Cardiovasc Res 29:260–268.

Sheldon C, Church J (2002) Intracellular pH response to anoxia in acutely dissociated adult rat hippocampal CA1 neurons. J Neurophysiol 87:2209–2224.

Sheldon C, Church J (2004) Reduced contribution from Na^+/H^+ exchange to acid extrusion during anoxia in adult rat hippocampal CA1 neurons. J Neurochem 88:594–603.

Sheldon C, Diarra A, Cheng YM, Church J (2004) Sodium influx pathways during and after anoxia in rat hippocampal neurons. J Neurosci 24:11057–11069.

Shrode LD, Putnam RW (1994) Intracellular pH regulation in primary rat astrocytes and C6 glioma cells. Glia 12:196–210.

Stys PK (2004) White matter injury mechanisms. Curr Mol Med 4:113–130.

Stys PK (2005) General mechanisms of axonal damage and its prevention. J Neurol Sci 233:3–13.

Su G, Kintner DB, Sun D (2002) Contribution of $Na^+K^+Cl^-$ cotransporter to high $[K^+]_o$-induced swelling and EAA release in astrocytes. Am J Physiol Cell Physiol 282:C1136–C1146.

Suzuki Y, Matsumoto Y, Ikeda Y, Kondo K, Ohashi N, Umemura K (2002) SM-20220, a Na(+)/H(+) exchanger inhibitor: effects on ischemic brain damage through edema and neutrophil accumulation in a rat middle cerebral artery occlusion model. Brain Res 945:242–248.

Swanson RA, Shiraishi K, Morton MT, Sharp FR (1990) Methionine sulfoximine reduces cortical infarct size in rats after middle cerebral artery occlusion. Stroke 21:322–327.

Teshima Y, Akao M, Jones SP, Marban E (2003) Cariporide (HOE642), a selective Na^+-H^+ exchange inhibitor, inhibits the mitochondrial death pathway. Circulation 108:2275–2281.

Tombaugh GC, Sapolsky RM (1993) Endocrine features of glucocorticoid endangerment in hippocampal astrocytes. Neuroendocrinology 57:7–13.

Xia Y, Zhao P, Xue J, Gu XQ, Sun X, Yao H, Haddad GG (2003) Na^+ channel expression and neuronal function in the Na^+/H^+ exchanger 1 null mutant mouse. J Neurophysiol 89:229–236.

Xue J, Douglas RM, Zhou D, Lim JY, Boron WF, Haddad GG (2003) Expression of Na^+/H^+ and HCO_3^- -dependent transporters in Na^+/H^+ exchanger isoform 1 null mutant mouse brain. Neuroscience 122:37–46.

Yamamoto S, Matsui K, Ohashi N (2002) Protective effect of Na^+/H^+ exchange inhibitor, SM-20550, on impaired mitochondrial respiratory function and mitochondrial Ca^{2+} overload in ischemic/reperfused rat hearts. J Cardiovasc Pharmacol 39:569–575.

Yao H, Ma E, Gu XQ, Haddad GG (1999) Intracellular pH regulation of CA1 neurons in Na(+)/H(+) isoform 1 mutant mice. J Clin Invest 104:637–645.

Yao H, Gu XQ, Douglas RM, Haddad GG (2001) Role of Na^+/H^+ exchanger during O_2 deprivation in mouse CA1 neurons. Am J Physiol Cell Physiol 281:C1205–C1210.

Zhou D, Xue J, Gavrialov O, Haddad GG (2004) Na^+/H^+ exchanger 1 deficiency alters gene expression in mouse brain. Physiol Genomics 18:331–339.